Genome Biology

Open Access

Pamoic acid and carbenoxolone specifically inhibit CRISPR/Cas9 in bacteria, mammalian cells, and mice in a DNA topology-specific manner

Yuxuan Zhang[1], Wentao Zou[1], Yueyang Zhou[1], Jiaqi Chen[1], Youtian Hu[1] and Fang Wu[1*]

*Correspondence:
fang.wu@sjtu.edu.cn

[1] Key Laboratory of Systems
Biomedicine (Ministry
of Education), Shanghai Center
for Systems Biomedicine,
Shanghai Jiao Tong University,
Shanghai 200240, China

Abstract

Background: Regulation of the target DNA cleavage activity of CRISPR/Cas has naturally evolved in a few bacteria or bacteriophages but is lacking in higher species. Thus, identification of bioactive agents and mechanisms that can suppress the activity of Cas9 is urgently needed to rebalance this new genetic pressure.

Results: Here, we identify four specific inhibitors of Cas9 by screening 4607 compounds that could inhibit the endonuclease activity of Cas9 via three distinct mechanisms: substrate-competitive and protospacer adjacent motif (PAM)-binding site-occupation; substrate-targeting; and sgRNA-targeting mechanisms. These inhibitors inhibit, in a dose-dependent manner, the activity of *Streptococcus pyogenes* Cas9 (*Spy*Cas9), *Staphylococcus aureus* Cas9 (*Sau*Cas9), and *Spy*Cas9 nickase-based BE4 base editors in in vitro purified enzyme assays, bacteria, mammalian cells, and mice. Importantly, pamoic acid and carbenoxolone show DNA-topology selectivity and preferentially inhibit the cleavage of linear DNA compared with a supercoiled plasmid.

Conclusions: These pharmacologically selective inhibitors and new mechanisms offer new tools for controlling the DNA-topology selective activity of Cas9.

Keywords: Anti-CRISPR, Selective small-molecule inhibitors, Mode of action, DNA topology, Mice model of hydrodynamic injection

Background

Type II CRISPR/Cas9 is the earliest identified, most widely used, and simplest genetic tool for genome editing in bacteria and mammalians [1, 2]. It only requires a single Cas9 protein with two endonuclease domains (RuvC and HNH) and a ~ 20-bp nucleotide recognizing single-strand guide RNA (sgRNA) to locate and double-cut the two strands of target DNA from millions of nucleotides within minutes [1, 3]. The accurate positioning mechanism of CRISPR was found to rely not only on the matching of RNA to DNA, but also on

the recognition between the PI domain (also known as topoisomerase-homology and the C-terminal domain) [3–5] and the downstream protospacer adjacent motif (PAM), which is a conserved motif that discriminates between self and non-self DNA [6].

Although CRISPR has been successfully applied throughout the genomes of various organisms, including humans, genotoxicity and off-targeting effects, as well as other safety issues, have been frequently observed and warned [7–10]. Therefore, spatiotemporal control and elimination of the unwanted activity of CRISPR gene editing are needed [11]. Pioneering studies have shown that naturally occurring anti-CRISPR proteins or peptides are employed by phages or bacterial hosts to suppress the activity of CRISPR by interfering with the loading of sgRNA, competing with the binding of DNA, or inhibiting the cleavage activity of endonuclease domain [12–15]. Recently, AcrIIA4, an anti-CRISPR protein for *Streptococcus pyogenes* Cas9 (*Spy*Cas9) [13, 16], was used to switch off the activity of *Spy*Cas9 in vivo [17]. Small-molecule inhibitors targeting Cas9 have been successfully discovered to suppress the gene-editing activity of Cas9 in an in vitro purified enzyme assay and in mammalian cells [18, 19], proving a proof-of-concept for the competency of chemical inhibitors on the activity regulation of genome-editing enzymes. However, the discovery of small-molecule inhibitors lags immensely behind that of anti-CRISPR proteins, not only in number but also in mechanistic insight and application scope. Moreover, since the transition state or the detailed mechanism for Cas9 cleaving the DNA strands is not fully understood yet [20], the discovery of small-molecule inhibitor that could stabilize either catalytic step of Cas9 will facilitate the determination of the structure of Cas9-DNA cleavage complex and its catalytic mechanism.

In the present study, we identified 31 compounds that dose-dependently inhibited the endonuclease activity of purified *Spy*Cas9 or *Staphylococcus aureus* Cas9 (*Sau*Cas9); four of these compounds, i.e., pamoic acid, dalbavancin, carbenoxolone, and epirubicin, potently blocked bacterial or mammalian genome editing mediated by *Spy*Cas9, *Sau*Cas9, or BE4 base editors at multiple endogenous loci. Moreover, pamoic acid and carbenoxolone leads, which display a substrate-competitive and PAM-binding site-occupation mechanism, selectively inhibited the cleavage of linear DNA compared with that of supercoil DNA by Cas9. Importantly, pamoic acid, carbenoxolone, and dalbavancin can pharmacologically modulate Cas9-mediated genome editing in mice.

Results

Identification of FDA-approved drugs as new Cas9 inhibitors by enzymatic activity assays

After optimizing the activity assay of *Spy*Cas9 (Additional file 1: Fig. S1A-D) [1], we performed primary screening to identify inhibitors from 4607 Food and Drug Administration (FDA) or Foreign Approved Drugs (FAD)-approved drugs or natural products at 200 μM, with a circular green fluorescent protein (GFP) plasmid as a substrate (Fig. 1A). It is noteworthy to point out that the linear form of the GFP plasmid (∼7200 bp) migrates faster than the covalently closed circular DNA (cccDNA) form of the plasmid in the DNA agarose gel electrophoresis using Tris borate EDTA (TBE) running buffer, a phenomenon that was previously reported for the migrations of plasmid at this size and in the TBE buffer [21]. Additionally, we have verified the migrating position for the

Zhang *et al. Genome Biology*   (2025) 26:75

Page 3 of 38

linear form of GFP plasmid by incubating the plasmid with EcoRI restriction enzyme in the absence of *Spy*Cas9 and sgRNA (Additional file 1: Fig. S1B).

Thirty-one compounds were found to dose-dependently inhibit the in vitro DNA-cleavage activity of *Spy*Cas9 with IC_{50} values of less than 200 µM by using the plasmid and/or an 87 bp linear oligonucleotide as a substrate (Additional file 1: Table S1 and Fig. S2; see the "Methods" section). Notably, these hits can be classified into eight categories with different molecular functions but similar structures within the class [24–55]. The best hit from categories I to VI displayed more pronounced inhibition of *Spy*Cas9 activity, i.e. having IC_{50} values of ~ 20 µM or less, and a specific mode of action (Table 1, Additional file 1: Table S1 and Fig. 1A). Considering the modes of action of the six hits, we ultimately removed the bleomycin inhibitor (category II), which is a DNA and chromosome damage agent [29], and selected the remaining five leads for subsequent investigation: i.e., epirubicin (topoisomerase inhibitor), dalbavancin (an inhibitor of cell wall synthesis of gram-positive bacteria), oxantel pamoate

(See figure on next page.)

Fig. 1 The primary inhibitor screening and identification of FDA-approved drugs to inhibit the endonuclease activity of Cas9 with a purified enzyme-based activity assay. **A** The primary inhibitor screening for suppressing the endonuclease activity of SpyCas9 and the schematic diagram for the in vitro enzyme assay, bacteria, mammalian cells, or animal -based studies of Cas9 inhibitors. After a drug screening of 4607 compounds at 200 µM in the activity assay of Cas9, 31 compounds were found to dose-dependently inhibit the activity of Cas9 with IC_{50} values less than 200 µM. Five representative leads were selected for the efficacy and selectivity studies on purified enzyme, bacteria, mammalian cell or animal levels. **B** The effect of five leads as well as AcrIIA4 on the cleavage activity of *Spy*Cas9 to the circular plasmid. Pamoic acid, epirubicin, dalbavancin, carbenoxolone or docusate at the indicated concentrations was incubated with a complex of *Spy*Cas9 (375 nM) and sgRNA (400 nM) and tested under the standard assay conditions (Additional file 1:Fig. S1B-C;see the "Methods" section). The pcDNA3.1/CT-*GFP* plasmid (300 ng) containing a protospacer sequence (N20: 5'-CCAATTCTTGTTGAATTAGA-3') and a 5'-TGG PAM (Additional file 1: Table S4) was used in the assay. AcrIIA4, a known anti-CRISPR protein inhibitor of Cas9 [22], was also tested under the standard assay conditions with an exception of using 22 °C for the assay instead of 37 °C, which was reported for AcrIIA4 to show a better inhibition to *Spy*Cas9 [23]. In TBE buffer, the linear form of pcDNA3.1/CT-*GFP* plasmid (~ 7200 bp) migrates faster than the covalently closed circular DNA (cccDNA) form of the plasmid, which was reported previously [21] and also validated by us (Additional file 1:Fig.S1B).Means ± SDs (*n* = 3, biological replicates). **C** The effect of five leads as well as AcrIIA4 on the cleavage activity of SpyCas9 to the linear oligonucleotide substrate. Pamoic acid, epirubicin, dalbavancin, carbenoxolone, or docusate as well as AcrIIA4 was tested under the assay conditions described above (**B**) using a FAM-labeled 87 bp oligonucleotide as the substrate (10 nM; linear substrate, thereafter), which bears the same sequence of protospacer and PAM to the pcDNA3.1/CT-*GFP* plasmid (**B**). Eighty seven base pairs, the 5′-FAM-labeled substrate. Thirty base pairs, the FAM-labeled cleaved 5′-terminal fragment. Means ± SDs (*n* = 3, biological replicates). **D,E** The effect of five leads on the enzymatic activity of SauCas9. Pamoic, epirubicin, dalbavancin, carbenoxolone, or docusate at the indicated concentrations were incubated with the complex of SauCas9 (100 nM) and sgRNA (100 nM) before the addition of the pcDNA3.1/CT-*GFP* plasmid (300 ng, **D**) or a FAM-labeled 87 bp oligonucleotide (10 nM, **E**). The two forms of DNA substrate of this assay share the same sequence of protospacer (N21, 5′-CTGGAGTTGTCCCAATTCTTG-3′) and 5′-TTGAAT PAM (Additional file 1: Table S4). The original images for circular plasmid and linear oligonucleotide are shown in the Additional file 1: Fig. S3F and S3G, respectively. Means ± SDs (*n* = 3, biological replicates). DNA only, pcDNA3.1/CT-*GFP* plasmid (**B**), or 87 bp linear DNA (**C**) in the presence of assay buffer (see the "Methods" section). The optical density of the DNA band for the linear form (agarose gels, **B**) or for the 30 bp product (polyacrylamide gels, **C**), as well as the area containing the linear, open circular, and supercoil bands of the plasmid (**B**) or the area containing the 87 bp and 30 bp products (**C**) was quantified using ImageJ software (NIH, Bethesda, MD). The cleavage activity of Cas9 was calculated by dividing the band density of the linear form (**B**) or 30 bp product (**C**) by the density of total area in the same lane (100%) and is shown as a percentage below the gel. The cleavage activity was normalized to that of the DMSO group (100%), as shown in the right panel. Statistical analysis was performed using one-way ANOVA with Tukey's multiple comparisons test; *$p < 0.05$; **$p < 0.01$; ***$p < 0.001$. The experiments were independently repeated three times, and representative results are presented
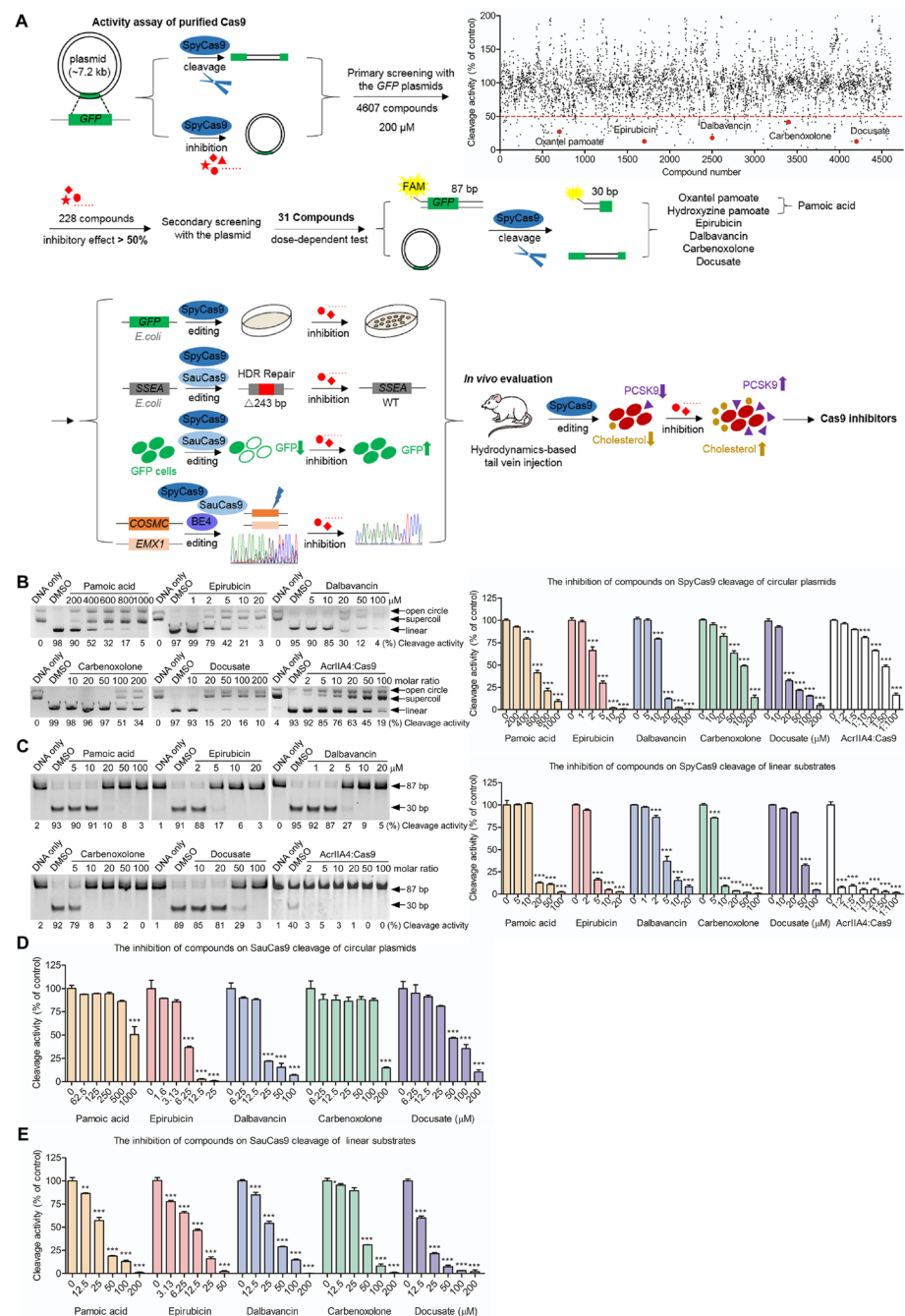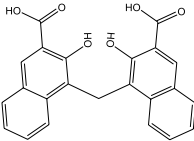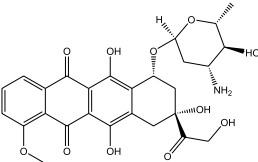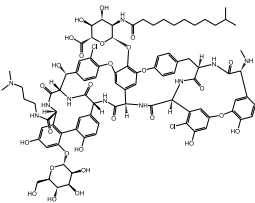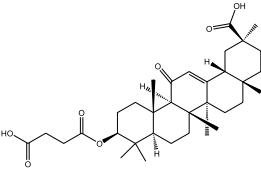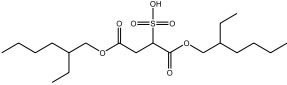
Fig. 1 (See legend on previous page.)

(anti-parasitic agent), carbenoxolone (an inhibitor of human or bacterial hydroxysteroid dehydrogenases), and docusate (a stool softener and surfactant) [38–40, 42, 45, 56, 57]. Epirubicin and dalbavancin were the most effective Cas9 inhibitors, with IC_{50} values of ~2–5 µM and 10–20 µM for plasmid cleavage (Fig. 1B) or ~2–5 µM and ~5 µM for linear oligonucleotides (Fig. 1C), respectively. The other three compounds, oxantel pamoate, carbenoxolone, and docusate, displayed weaker IC_{50} values ranging

Table 1 The structure and inhibitory effect of representative Cas9 inhibitors

Name & Use	Structure	IC$_{50}$ (µM)			
		Type of Cas9	In vitro purified enzyme assay	Bacteria-based assay	Cell-based assay
Pamoic acid (common component of oxantel pamoate and hydroxyzine pamoate)		*Spy*	400–600[a] 10–20[b]	200–400[c] ~ 400[d]	20–50[e] 20–50[f] ~ 50[g]
		Sau	500–1000[a] 25–50[b]	250–500[d]	20–50[f]
Epirubicin (topoisomerase II inhibitor)		*Spy*	2–5[a] 2–5[b]	3.13–6.25[c] 6.25–12.5[d]	-
		Sau	3.13–6.25[a] 6.25–12.5[b]	~ 6.25[d]	-
Dalbavancin (cell wall synthesis inhibitor & Gram-positive bacteria inhibitor)		*Spy*	10–20[a] ~ 5[b]	12.5–25[c] 6.25–12.5[d]	~ 10[e] ~ 10[f] ~ 10–20[g]
		Sau	12.5–25[a] ~ 25[b]	12.5–25[d]	~ 10[f]
Carbenoxolone (human or bacterial hydroxysteroid dehydrogenase inhibitor)		*Spy*	~ 100[a] 5–10[b]	~ 200[c] 50–100[d]	10–20[e] 20–50[f] 20–50[g]
		Sau	100–200[a] 25–50[b]	100–200[d]	20–50[f]
Docusate (stool softener and surfactant)		*Spy*	10–20[a] 20–50[b]	-	-
		Sau	25–50[a] 12.5–25[b]	-	-

[a] Supercoil plasmids

[b] Linear substrates

[c] The bacterial survival assay using pCas and pTarget-sg*SSEA* plasmids

[d] PCR-based genotyping assay for analyzing the *SSEA* site in MG1655 with pCas9 or pCas9-*Sau* and pTarget-sg*SSEA* (867 bp) in the presence of an HDR repair template

[e] GFP-disruption assay using the PX459-*Spy*Cas9 and pGL3-sg*GFP* plasmids

[f] TIDE analysis, editing efficiency for *COSMC* or *EMX1* loci in HEK293FT cells

[g] BE4 base editing efficiency for *EMX1* loci

from 20 to 50 µM, with the exception of carbenoxolone on linear DNA (IC$_{50}$ ~ 5−10 µM) (Fig. 1B,C, Table 1 and Additional file 1: Fig. S2).

Strikingly, oxantel pamoate and hydroxyzine pamoate, another newly identified Cas9 inhibitor within this class (Additional file 1: Table S1), showed a more pronounced potency to preferentially inhibit the hydrolysis of linear DNA (IC$_{50}$ ~ 20−50 µM) rather

than that of the circular plasmid ($IC_{50} > 200$ μM) (Additional file 1: Fig. S3A). However, pamoic acid, a common component of oxanthine pamoate and hydroxyzine pamoate [40, 41], was found to be responsible for this inhibition and selectivity. Pamoic acid, rather than hydroxyzine (Additional file 1: Fig. S3B), the other ingredient of hydroxyzine pamoate, potently inhibited the cleavage of an 87-bp linear oligonucleotide or 2.5 kb linear DNA ($IC_{50} \sim 10–20$ μM), but weakly affected the circular plasmid ($IC_{50} \sim 600$ μM) (Fig. 1B,C and Additional file 1: Fig. S3C). Carbenoxolone and AcrIIA4, the latter of which is a known anti-Cas9 peptide inhibitors [13, 16], recoined this selectivity between the linear and circular DNA (Fig. 1B,C), suggesting this uncovered phenomenon may exist universally.

To verify these findings, we tested the inhibitory effect of these five leads on the activity of purified *Sau*Cas9 (Additional file 1: Fig. S3D), which is homologous to *Spy*Cas9 and belongs to the same Type II-A subclass [58], in the presence of a circular *GFP* plasmid or an 87-bp linear oligonucleotide, under established assay conditions (Additional file 1: Fig. S3E). Consistently, epirubicin and dalbavancin remained potent inhibitors to *Sau*Cas9 with similar IC_{50} values of 6.25–12.5 μM and 12.5–25 μM, respectively, regardless of the topology of DNA substrate (Fig. 1D,E and Additional file 1: Fig. S3F-G). Also, BRD0539, the known inhibitor of *Spy*Cas9 that is with an IC_{50} value of 22 μM in the in vitro DNA cleavage assay [18], was found to inhibit the ability of *Sau*Cas9 to cleave circular plasmid and linear DNA with IC_{50} values of ~ 50 μM and 10–20 μM, respectively (Additional file 1: Fig. S3H), suggesting that the small molecule inhibitor of *Spy*Cas9 could inhibit other Cas9 orthologs in the same subtype.

Moreover, pamoic acid and carbenoxolone potently inhibited the cleavage of the linear substrate rather than circular DNA by *Sau*Cas9 at low micromolar concentrations ($IC_{50} \sim 25–50$ μM; (Fig. 1D,E and Additional file 1: Fig. S3F-G). Importantly, these inhibitors, as well as AcrIIA4, potently inhibited the cleavage of DNA by commercially available Cas9 and maintained their selectivity between the circular plasmid and linear DNA (Additional file 1: Fig. S4A).

Collectively, we identified five new inhibitors that potently suppress the activities of *Spy*Cas9 and *Sau*Cas9 via in vitro purified enzyme assays.

The biochemical basis for the inhibition of Cas9 activity by five representative leads

First, all the compounds seemed to act in a reversible manner to inhibit the activity of *Spy*Cas9 when pre-incubation with *Spy*Cas9 or with catalytically dead *Spy*Cas9 (dCas9) apoprotein (Additional file 1: Fig. S4B-C), and four leads, that is, pamoic acid, dalbavancin, carbenoxolone, and docusate, were found to have reasonable binding affinities for the *Spy*Cas9 enzyme (K_D values from 12.8 to 56.4 μM) (Fig. 2A and Additional file 1: Fig. S4D) comparable to their respective IC_{50s} (from 5 to 50 μM; Table 1). However, epirubicin hardly bound to *Spy*Cas9 at low micromolar concentrations ($K_D > 1$ mM) (Additional file 1: Fig. S4D), which did not correspond to its most pronounced IC_{50} value (2–5 μM) among these leads (Table 1) and suggested its inhibition on the catalytic activity of Cas9 is not via directly targeting the Cas9 protein.

Moreover, pre-incubation of pamoic acid or carbenoxolone with *Spy*Cas9 before the addition of the DNA substrate seemed to increase their inhibitory potencies in the enzymatic assay (Fig. 2B) but did not affect the IC_{50s} of the other three

compounds (Additional file 1: Fig. S4E). In addition, pamoic acid or carbenoxolone dose-dependently dissociated the complex formed with the dCas9 ribonucleoprotein and the linear oligonucleotide or circular *GFP* plasmid substrate in the electrophoretic mobility shift assays (EMSA) (Fig. 2C). This substrate-competitive effect was previously reported and was observed for AcrIIA4 in our EMSA assay (Additional file 1: Fig. S4F) [13, 16]. However, the binding of inhibitors to Cas9 did not seem to require the presence of sgRNA, as reflected by pamoic acid or carbenoxolone, which still disrupted the binding of dCas9 protein to the plasmid or 87 bp linear DNA in the absence of sgRNA (Fig. 2C-D). In sharp contrast, dalbavancin did not prevent the binding of DNA substrates to the dCas9 ribonucleoprotein or dCas9 itself (Fig. 2C,D, Additional file 1: Fig. S4G). Instead, dalbavancin could bind to the

(See figure on next page.)

Fig. 2 The biochemical mechanisms of five representative leads on inhibiting *Spy*Cas9. **A** Surface plasmon resonance assay analysis of the binding of five representative leads to *Spy*Cas9. *Spy*Cas9 at a concentration of 100 µg/mL was immobilized onto the surface of the CM5 sensor chip and then employed to analyse the binding of pamoic acid, dalbavancin or carbenoxolone as well as epirubicin and docusate (Additional file 1:Fig. S4D). The equilibrium affinity constant (K_D) values were calculated with BIAcore evaluation software (version 3.1). **B** The pre-incubation of pamoic acid or carbenoxolone, but not dalbavancin, epirubicin or docusate, with *Spy*Cas9 ribonucleoprotein enhances their inhibitory effects on the activity of Cas9. Pamoic acid or carbenoxolone at the indicated concentrations were pre-incubated with Cas9: sgRNA (375 nM: 400 nM) for 15 min before adding the *GFP* plasmid (condition **a** of left panel), or exposed to the enzyme together with the plasmid without a pre-incubation (condition **b**). Then, the samples were tested under the standard assay conditions. Means ± SDs ($n = 3$, technical replicates). The results for other inhibitors were slowed in the Additional file 1: Fig. S4E. **C-D** Pamoic acid or carbenoxolone, but not dalbavancin, docusate or epirubicin, specifically prevents the binding of DNA substrate to *Spy*Cas9 in DNA EMSA assays. dCas9 in the presence of sgRNA (**C** or right panelof **D**) or in the absence (left panelof **D**) was incubated with the 5'-FAM labeled linear DNA substrate or plasmid and the inhibitor under the indicated sampling order, before a separation on a 6% native polyacrylamide gel (upper panel of **C** for the 87 bp oligonucleotide; see the"Methods" section) or a 1% native agarose gel (lower panel of **C** for the plasmid). The polyacrylamide gels were stained with 1 × SYBR™ Gold (the right panel of **C** and **D**) or were imaged for fluoresence of FAM under an excitation of 488 nm on a ChemiDoc scanner (left and upper panels of **C**; left panel of **D**), while the agarose gel was dying with EB and illuminated under UV (lower panels of **C**). The lower and right panel of **C**, the plasmid DNA (the lower and left panel) treated with the indicated compounds in the absence of dCas9 and sgRNA. **E** Dalbavancin binds to free sgRNA or dCas9: sgRNA complex in a sgRNA EMSA assay. The free sgRNA (left panel) or sgRNA captured with dCas9 (right panel) was incubated with the inhibitor before a staining with 1 × SYBR™ Gold. **F** Epirubicin as well as doxorubicin or cisplatin directly binds to free DNA substrates. The plasmid (300 ng, equal to 5 nM) or oligonucleotide (10 nM) was pre-incubated with the compounds before adding of 5 × loading buffer containing 1.2% SDS. The samples were heated for 5 min at 95 °C and separated on respective gels (see above). **G** Oligonucleotide containing 8 × PAM rescues the destabilization of pamoic acid or carbenoxolone on Cas9 ribonucleoprotein in a thermal shift assay. The complex of Cas9 and sgRNA at 1 µM was incubated with 200 µM pamoic acid, 100 µM carbenoxolone or 50 µM dalbavancin for 15 min in the presence of the oligonucleotide containing of 8 × PAM at a molar ratio of 0.5:1, 1:1, 2:1 or 5:1 to Cas9 (see the "Methods" section). The melting curves of Cas9 were showed in the Additional file 1:Fig.S5D and the unfolding transition midpoint temperature (Tm) of Cas9 was calculated by the GraphPad software (version 8.4, San Diego, CA). Means ± SDs ($n = 3$, biological replicates). Statistical analysis was performed using one-way ANOVA with Tukey's multiple comparisons test; ns, no significance; **$p < 0.01$; ***$p < 0.001$. **H** The dose-dependent inhibitory effect of compounds on the cleavage of target strand ssDNA by Cas9. The activity assay was performed using 5'-FAM labeled 87 bp single stand oligonucleotide that is reverse and complement to the anti-*GFP* sgRNA and without the sequence of PAM (Additional file 1: Table S3-4), instead of the annealed double strand oligonucleotide. The original image was shown in the Additional file 1:Fig.S5F and the normalized data are shown here. Means ± SDs ($n = 3$, technical replicates). DNA only, pcDNA3.1/ CT-*GFP* plasmid (**B**, lower panel of **C** and upper panel of **F**), or 87 bp linear DNA (upper panel of **C, D** and lower panel of **F**) in the presence of assay buffer. The cleavage activity of Cas9 was determined and is shown as a percentage of the DMSO group (100%; right panel of **B** or **H**). All experiments were independently repeated at least twice, and representative results are presented
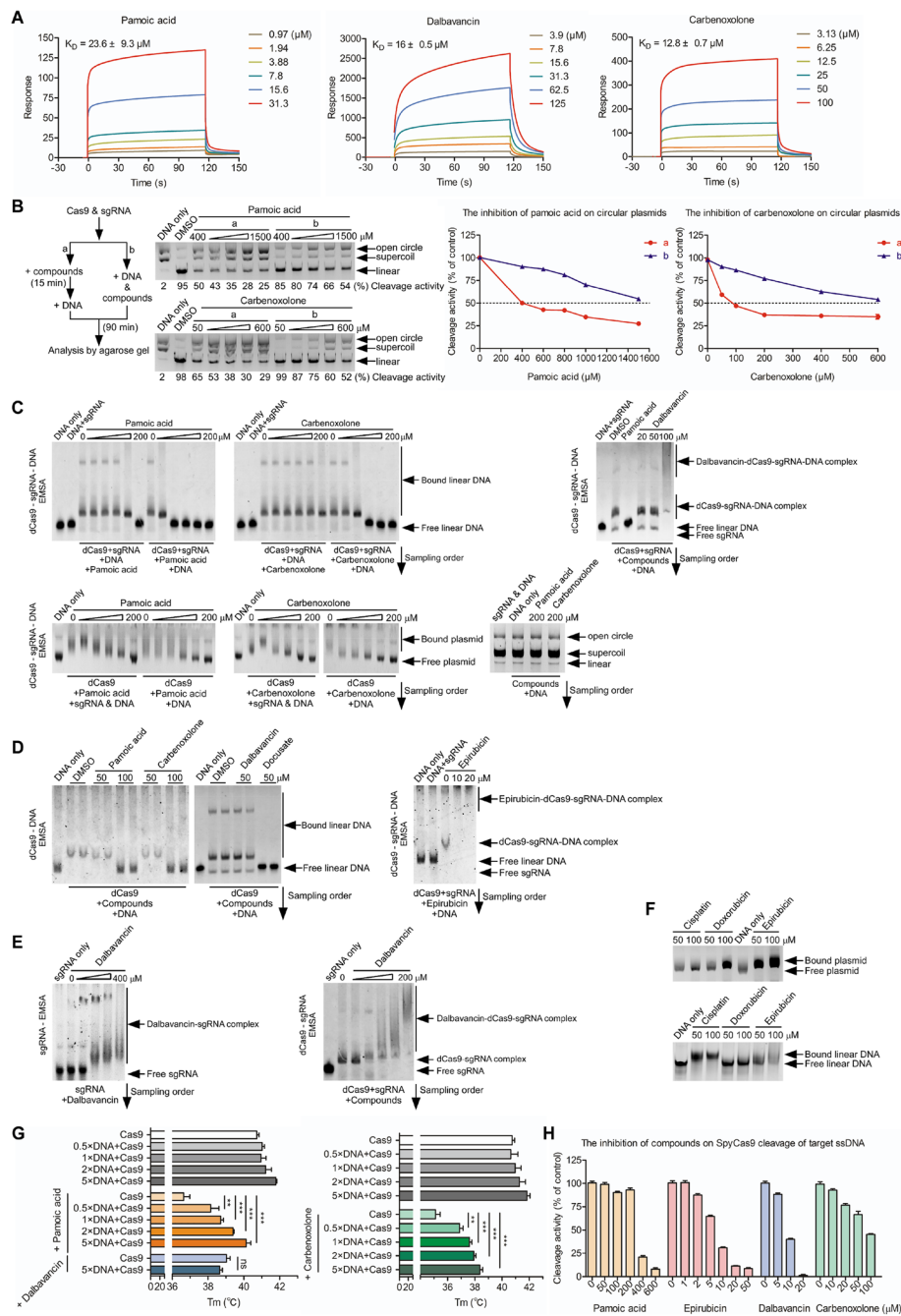
Fig. 2 (See legend on previous page.)

free sgRNA ribonucleotide or dCas9 ribonucleoprotein and trigger supershift bands of sgRNA (Fig. 2E and Additional file 1: Fig. S4H), offering an explanation to its inhibition on Cas9. Indeed, dalbavancin was found to irreversibly or tightly bind sgRNA and inhibit the activity of *Spy*Cas9, regardless of the presence or absence of Cas9, when dalbavancin was preincubated with Cas9: sgRNA ribonucleoprotein or with sgRNA first (Additional file 1: Fig. S4I). Intriguingly, dalbavancin was found to interact with the scaffold motif but not the spacer of the sg*GFP* (Additional file 1: Fig.

Zhang *et al. Genome Biology*   (2025) 26:75

Page 9 of 38

S5A). In addition, prime editing sgRNA (pegRNA) which contains the same scaffold sequence as *Spy*Cas9 sg*GFP* but has a different spacer sequence, indeed reacted with dalbavancin (Additional file 1: Fig. S5A) [59]. Moreover, disrupting the secondary structure of sg*GFP* with formamide seemed to inhibit the binding of dalbavancin (Additional file 1: Fig. S5B), suggesting dalbavancin may recognize the secondary structure of sgRNA regardless of the sequence of the spacer. However, the detailed inhibitory mechanism of dalbavancin needs to be explored in the future.

Notably, epirubicin, doxorubicin, and cisplatin, the other screening hits from the topoisomerase II (TOP II) inhibitor and DNA or RNA synthesis/repair inhibitor categories (Additional file 1: Table S1), were found to directly bind to the linear or plasmid substrate and cause a supershift in the naked DNA (Fig. 2F). Similar to the binding of dalbavancin to sgRNA, embedding of epirubicin did not interfere with the capture of Cas9 on the DNA substrate (Fig. 2D), while targeting the DNA substrate to block the catalytic activity of Cas9.

For docusate, the pre-addition of a DNA substrate could not rescue the disruptive effect of docusate on the complex association between dCas9 and DNA (Fig. 2D and Additional file 1: Fig. S5C), resulting in a plausible mechanism by which the compound does not specifically bind to the holo protein, which is supported by the original mode of action for docusate, that is, being a stool softener and surfactant (Table 1) [45].

In support of the DNA-competitive mechanism of pamoic acid or carbenoxolone, an incremental amount of DNA substrate containing a sequence of $8 \times$ PAM but without 20 nt protospacer (N20) [18] could dose-dependently prevent the decrease in melting temperature (Tm) caused by the treatment of pamoic acid or carbenoxolone in a thermal shift assay, with a maximum recovery ΔTm of 3.5 °C and 3.3 °C for pamoic acid and carbenoxolone, respectively (Fig. 2G and Additional file 1: Fig. S5D). This implies that pamoic acid or carbenoxolone competes with the binding of the PAM to the PI domain of Cas9, suggesting they are potential PAM-binding site-occupation inhibitors. However, it did not prevent the depressive effects of dalbavancin, which is a substrate-independent and sgRNA-dependent mechanism (see above). Consistently, pamoic acid and carbenoxolone but not dalbavancin or epirubicin, could compete with the $8 \times$ PAM DNA to bind dCas9 ribonucleoprotein (Additional file 1: Fig. S5E), suggesting they share the same binding site with the 5′-NGG PAM DNA. More specifically, pamoic acid or carbenoxolone, but not dalbavancin or epirubicin, seem to lose at least tenfold potency to inhibit the cleavage of target strand ssDNA ($IC_{50} > 200$ µM for pamoic acid and > 50 µM for carbenoxolone) (Fig. 2H and Additional file 1: Fig. S5F) compared with the dsDNA linear substrate (Table 1 and Fig. 1C), the former scenario of which does not need the presence of PAM and the formation of R-loop but preserves the downstream catalytic events of Cas9 [60]. This observation suggests that they may not inhibit downstream catalytic events of Cas9, but block the recognition between the 5′-NGG PAM of nontargeting strand and the PAM-interacting residues in *Spy*Cas9, such as, Arg1333 and Arg1335 [13, 16], or interfere with the unwinding of DNA duplex by Cas9 [4, 60].

Taken together, our data suggested that pamoic acid or carbenoxolone, dalbavancin, and epirubicin inhibited the activity of Cas9 via three distinct biochemical

Zhang *et al. Genome Biology*   (2025) 26:75

Page 10 of 38

mechanisms, i.e., substrate-competitive, sgRNA-targeting and substrate-targeting mechanisms, respectively.

The putative binding modes and structure activity relationship of substrate-competitive type of Cas9 inhibitors

Pamoic acid has two carboxylic groups segregated by seven carbon atoms (Table 1), resembling the pattern of the two carboxylic groups in the Asp69 and Glu70 residues of AcrIIA4, a mimic of PAM that binds to Arg1333 and Arg1335 of the PI domain (Additional file 1: Fig. S6A) [4, 16]. This unusual similarity led us to generate a putative binding mode for pamoic acid and carbenoxolone to *Spy*Cas9 using a structure-replacing and molecular simulation approach (Additional file 1: Fig. S6A). In support of the binding modes of the two inhibitors, their inhibitory potencies were found to decrease 5–10 folds on engineered *Spy*Cas9 variants Cas9-VQR (D1135V/R1335Q/T1337R) and SpRY-Cas9 [61, 62], compared with the IC_{50s} obtained from the 5′-NGG PAM and wt *Spy*-Cas9 (Fig. 3A, Fig. 1C and Additional file 1: Fig. S6B). The two Cas9 mutants target the 5′-NGA PAM and 5′ NHN PAM (H = A, C, or T) substrates and contain a mutation of R1335Q and a mutation combination of R1333P and R1335Q, respectively, which are the postulated binding sites for pamoic acid or carbenoxolone. Moreover, the reduction of the binding affinity of DNA competitor by using plasmids containing 5′-NAG or 5′-NGA PAM instead of 5′-NGG PAM, also potentiated the inhibitory effects of these inhibitors (IC_{50s} were found to decrease by 4–5 folds) (Fig. 3B and Additional file 1: Fig.

(See figure on next page.)

Fig. 3 The selectivity and structure–activity relationship of Cas9 inhibitor. **A** The effect of pamoic acid or carbenoxolone on inhibiting the activity of Cas9-VQR (upper) or SpRY-Cas9 (lower) mutant. Compounds were tested under the standard conditions with using the Cas9-VQR (D1135V/R1335Q/T1337R) or SpRY-Cas9 (A61R/L1111R/D1135L/S1136W/G1218K/E1219Q/N1317R/A1322R/R1333P/R1335Q/T1337R; NEB, M0669T) and the FAM-labeled 87 bp *GFP* oligonucleotide with a 5′-NGA or 5′-NAG PAM (Additional file 1: Table S2 and S4) [61], the latter of which is the preferred 5′-NHN PAM (H = A, C, or T) for SpRY-Cas9. The original images are shown in the Additional file 1: Fig. S6B. Means ± SDs ($n = 3$, biological replicates). **B** The effect of pamoic acid or carbenoxolone on inhibiting the cleavage of *GFP* plasmids containing a 5′-NAG or 5′-NGA PAM by *Spy*Cas9. The original images are shown in the Additional file 1: Fig. S6D. Means ± SDs ($n = 3$, technical replicates). **C** The effect of pamoic acid or carbenoxolone on the activity of *Spy*Cas9 nickase. Compounds were tested under the standard conditions using the wt *Spy*Cas9 or nickase, i.e. Cas9 D10A or Cas9 H840A mutant, and the linear *GFP* substrate. The original images were shown in the Additional file 1: Fig. S6E. Means± SDs ($n = 3$, biological replicates). **D** The structure-activity relationship of pamoic acid on inhibiting the activity of *Spy*Cas9 (see Additional file 1:Fig. S6F for the original images). The common structural moiety between the Asp60-Glu70 dipeptide (right panel) and pamoic acid is shown in orange. **E** The effect of compounds on the activity of *Fno*Cas12a or *Lba*Cas12a, Type V-A CRISPR/Cas enzyme with a respective 5′-TTN PAM and a 5′-TTTV PAM. The commercially available *Fno*Cas12a (left panel) or *Lba*Cas12a (right panel) CRISPR/Cas enzymes (#32106-03 or #32108-03 of ToloBio, Shanghai, China) were incubated with indicated compounds for 15 min before loading the pre-mixture of DNA substrate (DNA methyltransferase 1 fragment) and crRNA (see the "Methods" section). The 825 bp substrate or 525 bp and 300 bp products of DNA methyltransferase 1 was separated on 1% agarose gel and stained with EB. The optical density of the DNA bands was determined with ImageJ and the cleavage activity was showed as percentages ($n = 2$, biological replicates; see the "Methods" section). **F** The effect of Cas9 inhibitors on the activity of EcoRI or KpnI endonuclease. Compounds were tested in assays containing 375 nM Cas9 or 0.5 µl EcoRI or KpnI (7.5 U for EcoRI and 10 U for KpnI per assay) and 300 ng ~2.5 kb linear DNA (Additional file 1: Fig. S3C). The original images were shown in the Additional file 1: Fig. S7A. ATA, aurintricarboxylic acid [30] (Additional file 1: Table S1 and Additional file 1: Fig. S2). Statistical analysis was performed using one-way ANOVA with Tukey's multiple comparisons test; *$p < 0.05$; **$p < 0.01$; ***$p < 0.001$. All experiments were independently repeated at least twice, and representative results are presented
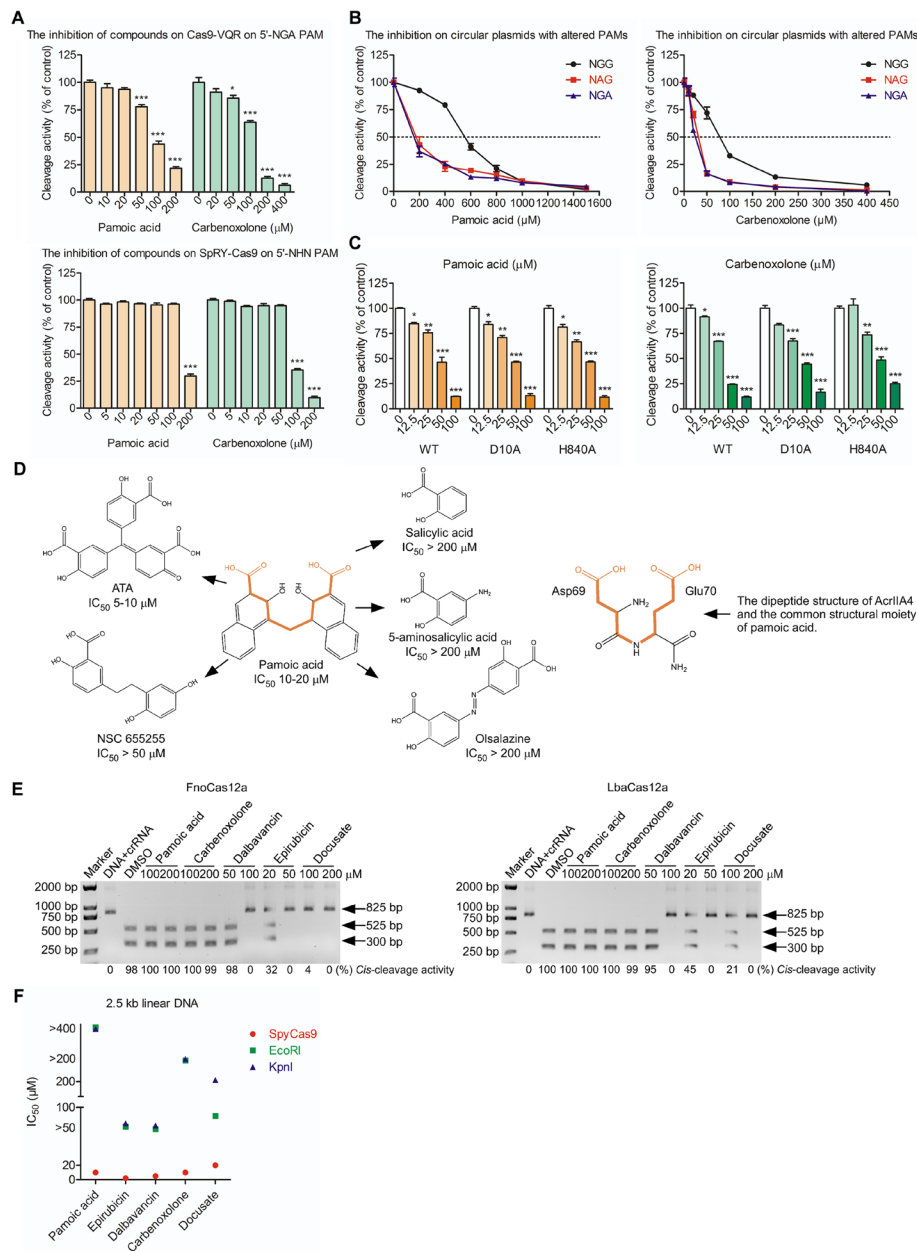
Fig. 3 (See legend on previous page.)

S6C-D). In sharp contrast, mutation of the catalytic residues D10 or H840 did not affect the IC_{50s} of pamoic acid or carbenoxolone, which are substrate-competitive and potential PAM-binding site-occupation inhibitors (Fig. 3C and Additional file 1: Fig. S6E). To this end, preliminary structure–activity relationship analysis for pamoic acid could potentially support the requirement for two carboxylic groups and their spanning distance, as compounds bearing one carboxylic group (salicylic acid or 5-aminosalicylic acid) or with a larger spanning distance (olsalazine or NSC655255) were inactive to Cas9 (Fig. 3D and Additional file 1: Fig. S6F).

Importantly, the 5′-NGG-PAM-recognition inhibitors pamoic acid and carbenoxolone as well as dalbavancin were inactive to or weakly inhibited *Francisella tularensis*

Zhang *et al. Genome Biology*   (2025) 26:75

Page 12 of 38

novicida Cas12a (*Fno*Cas12a) and *Lachnospiraceae bacterium* Cas12a (*Lba*Cas12a), two Type V CRISPR/Cas recognizing 5′-TTN and 5′ TTTV PAMs [63], respectively, whereas epirubicin or docusate did completely inhibit the activity at a concentration of 50 µM or above (Fig. 3E). Moreover, the substrate-competitive and substrate-targeting types of Cas9 inhibitors, as well as dalbavancin, the sgRNA-targeting inhibitor, but not the docusate, displayed more than 10 folds selectivity for other endonucleases, that is, EcoRI and KpnI, the activity of which does not require PAM or sgRNA (Fig. 3F and Additional file 1: Fig. S7A).

Overall, considering the inability of substrate DNA to compete for the binding of docusate to Cas9 (Fig. 2D and Additional file 1: Fig. S5C), and the limited selectivities of inhibition (less than 5 folds) between the Type II-A (*Spy*Cas9) and Type V (*Fno*Cas12a or *Lba*Cas12a) subtypes of CRISPR/Cas (Fig. 3E), and between the Cas9 and restriction enzymes (~ 5 folds; Fig. 3F), docusate was not selected for further studies.

New inhibitors with different mechanisms inhibit the genome editing of Cas9 in bacteria

To investigate whether pamoic acid, carbenoxolone, dalbavancin, or epirubicin which have different modes of action for inhibiting Cas9, are effective in bacteria, we first constructed and validated genome editing assays in the *E. coli* MG1655 strain (Fig. 4) based on the pCas and pTarget two-plasmid-based gene editing system for *E. coli* reported previously [64]. All compounds, as well as AcrIIA4, were found to inhibit the genome editing of *Spy*Cas9 on the endogenous *SSEA* gene, which encodes

(See figure on next page.)
Fig. 4 The effect of inhibitors on suppressing the genome editing on *SSEA* locus by *Spy*Cas9 or *Sau*Cas9 in bacteria. **A** The schematic diagram of two-plasmid-based bacterial survival assay for detecting the activity of *Spy*Cas9 in bacteria. pCas plasmid (Addgene #62225,Additional file 1: Table S2) was transformed into the *E. coli* MG1655 before an electroporation with pTarget plasmids coding for sgRNA targeting *SSEA* (pT-sg*SSEA*, Additional file 1: Table S4) or empty vector (pT-sg*Control*; pTargetF, Addgene #62226). Then, the effect of compounds was evaluated by counting the number of survival colonies (see the "Methods" section). **B** The effect of Cas9 inhibitors on the activity of *Spy*Cas9 in the two-plasmid-based bacterial survival assay. Compounds were incubated with the electroporated bacteria (**A**) for 1.5 h at 32 °C before spreading on LB plates with kanamycin and spectinomycin antibiotics. After an overnight incubation, the image of cultured plate was taken (Additional file 1:Fig.S7D), and the number of colonies (indicated below the plate image) was quantified with a Colony Counter software (Tanon, China), and expressed as the percentages of their respective control at the same concentration (the pT-sg*Control* electroporated strain treated with the compound, 100%; Additional file 1:Fig.S7D). Means ± SDs (*n* = 3, biological replicates). Statistical analyses were performed using two-way ANOVA with Bonferroni posttests; *p < 0.05; **p < 0.01; ***p < 0.001. **C** The schematic diagram of the genome editing assay for monitoring the activity of *Spy*Cas9 or *Sau*Cas9 in the presence of homologous repair template DNA and in bacteria. pCas plasmid was first transformed into MG1655 strain before an electroporation to pTarget plasmids carrying a pair of homologous repair template DNA that is missing the 1-243 bp of *SSEA* gene (see the "Methods" section) and a coding sequence for *Spy*Cas9 or *Sau*Cas9 sgRNA (pT-sg*SSEA*(867 bp)). Then, the *E. coli* cells were incubated with the compounds before genotyping with PCR for analyzing the efficiency of genome editing at the *SSEA*. 909 bp, the size of PCR product from a strain, in which 1-243 bp of *SSEA* is missing; 1152 bp, the size of PCR product from a strain with wt *SSEA* gene. **D** The effect of Cas9 inhibitors on the genome editing activity of *Spy*Cas9 (left panel) or *Sau*Cas9 (right panel) in the presence of a homologous recombination repair template. Compounds were incubated with the electroporated bacteria (**C**) for 20 h at 32 °C, and the *SSEA* in the treated bacteria was amplified with PCR and analyzed on a 1% agarose. The original images for PCR-based genome typing were shown in the Additional file 1:Fig.S8B. Means ± SDs (*n* = 3, biological replicates). The ddH$_2$O (for dalbavancin or carbenoxolone) or DMSO (pamoic acid or epirubicin) treated groups, 100%. Statistical analysis was performed using one-way ANOVA with Tukey's multiple comparisons test; ***p < 0.001. All experiments were independently repeated at least twice, and representative results are presented

Fig. 4 (See legend on previous page.)
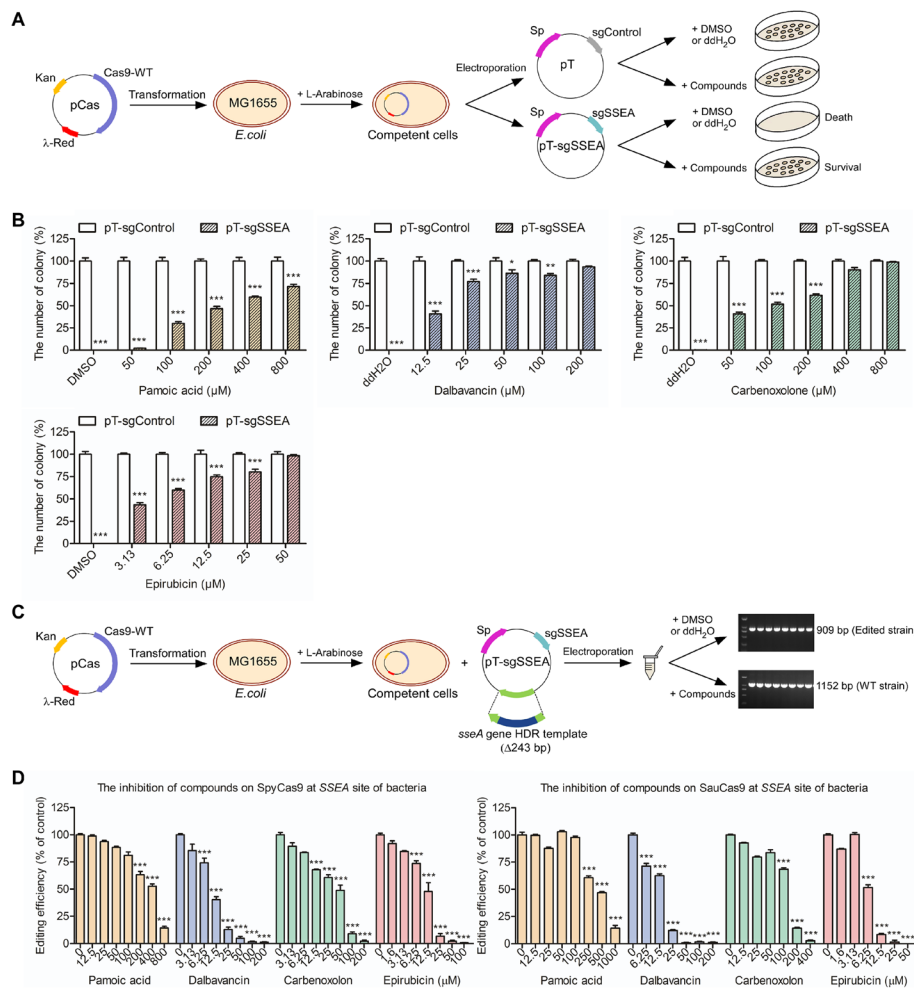
a 3-mercaptopyruvate sulfurtransferase enzyme [65], with a potency similar to that of the in vitro purified enzyme assay (Fig. 4A,B and Additional file 1: Fig. S7B-D). Epirubicin showed the most pronounced potency, with an IC_{50} value of ∼ 6.25 μM in the bacterial survival assay; however, it also had significant toxicity to electroporated bacteria at a concentration of 50 μM (Fig. 4B and Additional file 1: Fig. S7D-E). Pamoic acid, dalbavancin, and carbenoxolone seemed to have lower potency with IC_{50} values of ∼ 400, 12.5, and 100 μM, respectively, which corresponded to their inhibitory effects on the circular plasmid (Additional file 1: Fig. S7B and Fig. 1B). However, they did not appear to be much toxic to *E. coli* (Additional file 1: Fig. S7D-E), a gram-negative bacteria that is known not to respond to treatment with dalbavancin, a selective antibiotic for gram-positive bacteria [38, 39]. In addition, in the *SSEA* gene editing assay of *Spy*Cas9 or *Sau*Cas9, in the presence of a pair of homologous recombination repair templates missing 1–243 bp of *SSEA* gene (Δ243 bp), *Spy*Cas9 or *Sau*Cas9 could replace the wt *SSEA* gene (1152 bp) with the Δ243 bp *SSEA* gene (909 bp), the respective PCR products of which could be separated on agarose gels and the genotypes of the respective PCR products could be confirmed by DNA sequencing (Fig. 4C,D and Additional file 1: Fig. S8A-B). These compounds showed a comparable

potency in this assay to the bacterial survival assay that is in the absence of the repair template (Fig. 4A,B), indicating that the homology-directed repair step does not interfere with the mode of action of these compounds in bacteria.

Moreover, all four compounds could dose-dependently rescue bacterial survival in the plasmid-interference assay in the *E. coli* MG1655 strain transformed with *GFP* plasmids [14], indicating that they could prevent the gene editing of *Spy*Cas9 at the *GFP* site and in bacteria (Additional file 1: Fig. S8C-D). Together, these data showed that small molecule inhibitors of Cas9 could modulate the activity of Cas9 at the endogenous and exogenous gene sites in *E. coli.*

New inhibitors suppress the genome editing activity of SpyCas9, SauCas9, or SpyCas9 nickase-based BE4 base editor in mammalian cells

To test these new leads for inhibiting the activity of Cas9 in mammalian cells, we employed a green fluorescence protein (GFP)-based disruption assay that has been used for identification of Cas9 inhibitors (Fig. 5A) [18, 19]. All compounds showed dose-dependent inhibition of the endonuclease activity of Cas9 in scissoring an integrated *GFP* gene in HEK293FT cells, which was constructed using a lentivector containing the same DNA sequence of *GFP* as that used in the in vitro purified enzyme assay (Fig. 1 and see the "Methods" section). In the absence of a repair template, pamoic acid, dalbavancin, and carbenoxolone showed IC_{50s} of 20–50 μM, 10–20 and 10–20 μM (Fig. 5B and Additional file 1: Fig. S9A-B), respectively, which correspond to their activities on the linear substrate in the purified Cas9 enzyme assay (Fig. 1C).

Importantly, the inhibitory potencies of these compounds were maintained on the endogenous gene locus, that is, Core 1 β1–3 Galactosyltransferase Specific Molecular Chaperone (*COSMC*) or *EMX1*, as assessed by the Tracking of Indels by Decomposition (TIDE) or the next-generation sequencing method to quantify the templated editing PCR product, when the compounds were incubated with the cells at 0 or 6 h post-transfection of the PX459 plasmid containing Cas9 and sgRNA (Fig. 5C, Additional file 1: Fig. S9C-H or Additional file 1: Fig. S10A-C). Consistently, AcrIIA4 also broke the shearing of endogenous genes by Cas9 in these cellular assays (Additional file 1: Fig. S10D), and their inhibition was confirmed with an orthogonal analysis method, that is, a T7EI-based mismatch detection assay (Fig. 5D) [66]. Moreover, the inhibitory effect of these inhibitors seems to be consistent as reflected by a dose-dependent inhibition on the genome editing of *Spy*Cas9 in the HT29 cell line, a human colorectal adenocarcinoma cell line (Additional file 1: Fig. S10E). Of note, the three inhibitors, i.e., pamoic acid, carbenoxolone, and dalbavancin, but not epirubicin, were unable to induce genotoxicity in mammalian cells (Additional file 1: Fig. S10F). Moreover, these inhibitors at the highest concentration exposed to the cells did not cause substantial cytotoxicity or reduce the mRNA or protein level of Cas9, the former of which was carefully examined by using appropriate controls (Additional file 1: Fig. S11A-D). Taken together, these data verified that the inhibitors prevented gene editing by directly targeting Cas9 rather than by regulating its mRNA or protein, affecting the cell viability or causing genotoxicity.

Moreover, these compounds at these concentrations dose-dependently suppressed the base-editing activity of BE4, a Cytidine Base Editor that uses *Spy*Cas9 D10A nickase, a cytidine deaminase, and a protein inhibitor of base excision repair, to convert cytosine

to thymine at the 4th to 8th positions without breaking the double strands of DNA (Fig. 5E and Additional file 1: Fig. S11E-F) [70, 71]. In addition, the inhibitory effects on the conversion of C to T at the 5th or 6th position, away from the cleavage sites of Cas9 (between the 17th and 18th nucleotides), did not differ significantly from each other, suggesting that they may interfere with upstream events that require base editing, that

(See figure on next page.)

Fig. 5 The effect of inhibitors on suppressing the editing of exogenous *GFP* gene, endogenous *COSMC* or *EMX1* loci by *Spy*Cas9, *Sau*Cas9 or BE4 in HEK293FT cells. **A** The schematic diagram of cellular assays for analyzing the effects of inhibitors on the activity of *Spy*Cas9, *Sau*Cas9 or BE4 for the cleavage of *GFP*,*COSMC* or *EMX1* gene in HEK293FT cells. The cells were transfected with Lipofectamine™ 3000 Transfection Reagent (Thermal Fisher, L3000008) in the presence of plasmids containing *Spy*Cas9, *Sau*Cas9 or their sgRNAs before an incubation with the compound for 24 h. After the colony selection with puromycin, genomic DNA of the cells was then extracted, and the target gene was amplified with PCR (see the "Methods" section). The editing efficiency of Cas9 was analyzed with flow cytometry, TIDE, EditR or T7EI method [66–68]. **B** Flow cytometry analysis of the effect of compounds on the disruption of GFP by *Spy*Cas9 in HEK293FT cells. The cells stably expressing of GFP were transiently transfected with the PX459-*Spy*Cas9 (Addgene#62988) and pGL3 plasmids coding anti-*GFP* sgRNA (the blue line) or control sgRNA (the green line) before an incubation with the compound for 24 h (**A**). The GFP fluorescent from the treated cells was analyzed with LSR Fortessa flow cytometer (BD Biosciences, Franklin Lakes, NJ), and the gating strategy and corresponding histograms are shown in the Additional file 1:Fig.S9A-B. The quantitative data was shown as the percentage of the group treated with control sgRNA (100%). Means ± SDs ($n = 3$, biological replicates). **C** The effect of compounds on the editing of endogenous *COSMC* or *EMX1* by *Spy*Cas9 in HEK293FT wt cells. The cells were transfected with PX459-*Spy*Cas9 plasmid coding anti-*COSMC*, anti-*EMX1* sgRNA (for the spacer sequences, see Additional file 1: Table S4) or control sgRNA (the *Spy*Cas9 only group, Additional file 1:Fig.S9D),before the treatment with the indicated compounds for 24 h (**A**). The target DNA was accordingly amplified with PCR before subjected to Sanger sequencing (Additional file 1:Fig.S9E-Gand Additional file 1:Fig.S10A-C). The editing efficiency of Cas9 was analyzed with the TIDE method (https://tide.nki.nl/), normalized with the DMSO (for pamoic acid; final concentrations, 0.4%) or ddH$_2$O (for dalbavancin or carbenoxolone) -treated groups (100%) and shown. AcrIIA4 was used as a positive control (Additional file 1:Fig.S10D). Means ± SDs ($n = 3$, biological replicates). **D** T7EI mismatch detection assay analysis of the inhibitory effect of compounds on editing of *COSMC* by *Spy*Cas9 in HEK293FT cells. The amplified PCR products (541 bp; input) from the extracted genomic DNA of the control (the left four lanes of each gel) or edited HEK293FT cells (**C**), which have been treated with DMSO or ddH$_2$O (the middle four lanes), 100 µM pamoic acid, 50 µM dalbavancin or 50 µM carbenoxolone (the right four lanes), were incubated with T7EI or without the treatment at 37 °C for 15 min before an analysis the *COSMC* site with 2% agarose gels (see the "Methods" section). The percentage of Indel was calculated by the formula dividing the band density of fragments to that of total input and normalized with the background value [69]. **E** The effect of compounds on the base editing of *EMX1* by BE4 base editor in HEK293FT cells. The cells were co-transfected with the BE4 and pGL3 plasmids, the latter coding an anti-*EMX1* sgRNA that is the same as the one used for *Spy*Cas9 (Additional file 1: Table S4), and treated with the compounds for 24 h (**A**). The amplified PCR products from the *EMX1* site were accordingly sequenced (Additional file 1:Fig.S11E-F), and the converting rates of C_5 or C_6 base in the N20 sequence were analyzed with EditR (https://moriaritylab.shinyapps.io/editr_v10/;upperpanels) [66, 67]. The converting rate at the C_5 and C_6 position were normalized with the respective control (100%) and the base editing efficiency was shown as percentages for both the C_5 and C_6 sites (lower panels). Means ± SDs ($n = 3$, biological replicates). **F** The effect of compounds on the editing of *COSMC* by *Sau*Cas9 in HEK293FT cells. The cells were co-transfected with pX601-*Sau*Cas9 (Addgene #107055) and pGL3 plasmids containing an anti-*COSMC* sgRNA (Additional file 1: Table S2 and S4), before the treatment with the compounds for 24 h (**A**). The editing efficiency of Cas9 was analyzed with the TIDE method (https://tide.nki.nl/) and presented as percentages of control (100%). The raw sequencing results were shown in the Additional file 1:Fig.S12A-C. Means ± SDs ($n = 3$, biological replicates). **G** The comparison for the effects of pamoic acid or carbenoxolone on the *Spy*Cas9-mediated disruption of *GFP* plasmids with a 5′-NGG or 5′-NAG PAM. The HEK293FT wt cells were transiently co-transfected with the PX459-*Spy*Cas9 and pCDH-*GFP* plasmids, which contains a 5′-NGG PAM or an *in situ* mutated 5′-NAG PAM (see the "Methods" section) and were treated with the compounds 6 h post the transfection and for 24 h. The GFP fluorescent from the cells was accordingly quantified with flow cytometer and the data was shown as presentages of the control (100%; for the raw histograms, see Additional file 1:Fig.S12E; see the "Methods" section). Means± SDs ($n = 6$, biological replicates). Statistical analysis was performed using one-way ANOVA with Tukey's multiple comparisons test (**B**, **C**, **E** or **F**) or two-way ANOVA with Bonferroni posttests (**G**). *$p < 0.05$, **$p < 0.01$, ***$p < 0.001$. All experiments were independently repeated at least twice, and representative results are presented

Fig. 5 (See legend on previous page.)

is, the recognition of PAM and sgRNA, rather than strand-cleavage activity, deaminase activity, or the DNA repair cassette of non-homologous DNA end joining (NHEJ).

Conservatively, these inhibitors showed a similar potency on inhibiting the editing activity of *Sau*Cas9 at the *COSMC*, which targets a 5′-TAGGAT PAM at a position of the 80th bp of the *COSMC* gene (Fig. 5F and Additional file 1: Fig. S12A-C), when compared to the efficiency of *Spy*Cas9 designed for a 5′-TGG PAM at the 92th bp (Fig. 5C), suggesting their inhibition is independent of the protospacer sequence. In addition, we found that oxantel pamoate and hydroxyzine pamoate, two FDA-approved drugs, and

pamoic acid-containing compounds (Additional file 1: Table S1) inhibited *Spy*Cas9 or *Sau*Cas9 at the *COSMC* site with comparable efficiencies (Additional file 1: Fig. S12D). In contrast, pamoic acid or carbenoxolone, the potential PAM-recognition interfering inhibitor (Fig. 2 and 3), did show more pronounced inhibitory effect on the editing of the *GFP* plasmid with a 5′-NAG PAM or on that of known microfibrillar-associated protein 1 (*MFAP1*) and intergenic off-target sites of *EMX1* bearing a 5′-NAG PAM in cells (Fig. 5G or Additional file 1: Fig. S12E-F) [72, 73]. The latter showed a maximum increase of ∼ 2.5 folds in the targeting specificity of *Spy*Cas9 in a genome locus. These data suggested the two inhibitors could more favorably reduce the editing on this potential type of off-target site.

Altogether, these data proved that pamoic acid, carbenoxolone, and dalbavancin were bioactive inhibitors of *Spy*Cas9 and *Sau*Cas9, and they could dose-dependently inhibit the gene editing activity of Cas9 at various gene loci and/or reduce the off-target activity of Cas9 in mammalian cells.

New inhibitors dose-dependently prevent the genome editing of Cas9 in mice

To test the preventive effect of the compounds on Cas9-mediated genome editing in vivo, we established a *Spy*Cas9-mediated anti-protein convertase subtilisin/kexin type 9 (*PCSK9*) mouse model by hydrodynamic injection of an all-in-one Cas9-sgRNA plasmid (Fig. 6A), which has been successfully used to downregulate plasma levels of PCSK9 [74, 75]. After hydrodynamic injections of a PX459-*Spy*Cas9 plasmid containing a sgRNA targeting for mouse *PCSK9* at a 5′-AGG PAM site, a sgRNA which has been used previously and validated in our in vitro purified Cas9 assay with a 77-bp oligonucleotide substrate (Additional file 1: Fig. S13A) [76], the amount of plasma PCSK9 could be rapidly reduced by ∼ 50% 1 day post the 1st injection and maintain at the basal level after the 2nd or 3rd injections (Additional file 1: Fig. S13B and Fig. 6B). The pretreatment of the mice with pamoic acid is the only one that could completely restore the level of PCSK9 at the 1st, 2nd, or 3rd treatment cycle at a dose of 80 or 160 mg/kg and showed a

(See figure on next page.)

Fig. 6 The effects of inhibitors on antagonizing the Cas9-mediated genome editing in a hydrodynamic-injection-based anti-*PCSK9* mice model. **A** Scheme of experiments for the administration of compounds and construction of a *Spy*Cas9-mediated anti-*PCSK9* mouse model by hydrodynamic injection. BALB/c mice were intraperitoneally injected with the compounds at doses of 10, 20, 40, 80 or 160 mg/kg on day 0, followed by a hydrodynamic injection of 90 mμg of PX459-*Spy*Cas9 plasmids encoding anti-*PCSK9* sgRNA (Additional file 1: Table S4) [76] or control (vehicle group), and 5-8 s into the tail vein. Blood was collected via orbital bleeding on day 2. Two additional cycles of intraperitoneal injection of compounds (at the same dose as the 1st treatment), hydrodynamic injection of PX459-*Spy*Cas9 plasmids, or orbital bleeding to mice were performed on days 3-8 before the mice were sacrificed on day 8. **B** Pamoic acid, dalbavancin or carbenoxolone restored the circulatory amount of PCSK9 in a *Spy*Cas9-mediated anti-*PCSK9* mouse model. After collecting the blood sample from the orbital sinus on Day 2 (1st orbital blood collection), Day 5 (2nd orbital blood collection) or Day 8 (3rd orbital blood collection), the amount of plasma PCSK9 was determined by Mouse Proprotein Convertase 9/*PCSK9* Quantikine ELISA Kit (R&D, MPC900, Minneapolis, MN). Pamoic acid and dalbavancin were studied together in experiment 1, whereas carbenoxolone was studied in experiment 2. Means ± SDs (the groups of Cas9 + sg*PCSK9*+ saline and + 80 mg/kg pamoic acid in the 1st and 2nd treatment cycles of experiment 1, *n*= 12; the other groups, *n* = 6). Statistical analysis was performed using one-way ANOVA with Dunnett's multiple comparisons test (for the samples from 1st and 2nd treatment cycles of experiment 1) or with Tukey's multiple comparisons test (for the samples from the 3rd treatment cycles of experiment 1 and the samples from experiment 2). Ns, no significance; *$p < 0.05$; **$p < 0.01$; ***$p < 0.001$
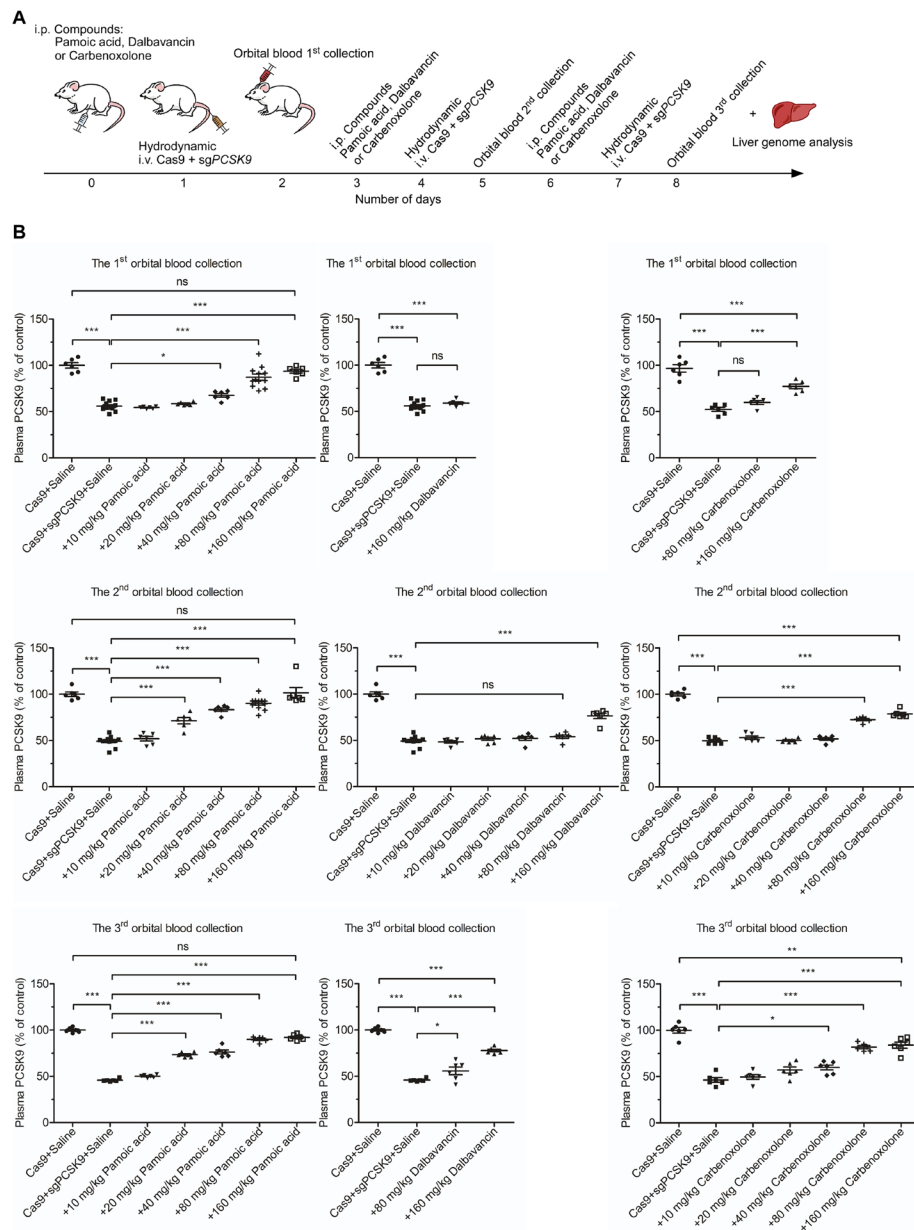
Fig. 6 (See legend on previous page.)

dose-dependent preventative effect starting from the 20 mg/kg dose (Fig. 6B). However, dalbavancin and carbenoxolone also had strong preventive effects at high doses of 80 or 160 mg/kg on the 2nd or 3rd treatment cycle, but not at low doses. In support of this, treatment with pamoic acid, dalbavancin, or carbenoxolone at a high dose of 160 mg/kg did not interfere with the basal level of PCSK9 in vehicle-treated mice (Additional file 1: Fig. S13C), suggesting that the rescuing effect of these inhibitors is indeed from conquering the activity of Cas9. Nevertheless, dalbavancin or carbenoxolone showed better inhibition ($IC_{50} \sim 5$ μM) on the cleavage of *PCSK9* by *Spy*Cas9 in vitro than did pamoic acid ($IC_{50} \sim 10$–20 μM; Additional file 1: Fig. S13A). Consistently, the editing efficiency and mutation types of *PCSK9* determined by analyzing the *PCSK9* loci of the liver

genome of 80 mg/kg pamoic acid or 160 mg/kg pamoic acid-treated mice with next-generation sequencing were completely reduced after three treatment cycles (Additional file 1: Fig. S13D-E), as reflected by the decreases in the percentages of reads modified and frequencies of allele modification to the basal level of ~ 0.5% or lower. Moreover, the treatment of pamoic acid at a medium dose of 40 mg/kg largely reduced but not totally prevented these allele modifications (Additional file 1: Fig. S13E). To this end, the plasma content of total cholesterol, a downstream effector of *PCSK9* [76], in the group treated with 80 mg/kg pamoic acid, 160 mg/kg pamoic acid, or 160 mg/kg carbenoxolone, but not with 40 mg/kg pamoic acid, 160 mg/kg dalbavancin, or 80 mg/kg carbenoxolone, was largely restored to the level of the control (Additional file 1: Fig. S13F), echoing the capacity of these compounds to restore the level of PCSK9 during the three treatment cycles (Fig. 6B).

These data showed that pamoic acid was the most active inhibitor for controlling the genome editing activity of Cas9 in mice, although dalbavancin and carbenoxolone were also found to be active at high doses.

Discussion

In the present study, we identified four FDA drugs as specific inhibitors of *Spy*Cas9 and *Sau*Cas9 by screening 4607 clinically approved agents or natural products using agarose gel-based DNA-cleavage Cas9 assays. These compounds selectively inhibited the endonuclease activity of Cas9 via three biochemical mechanisms: substrate-competitive (pamoic acid and carbenoxolone), substrate-targeting (epirubicin), and sgRNA-targeting (dalbavancin) (Fig. 7). Notably, the substrate-competitive mechanism has been selected by phages or bacteria to antagonize the defense of CRISPR/Cas; for example, AcrIIA4 occupies the PAM-binding pocket and thus prevents the binding of DNA to *Spy*Cas9 [13]. The substrate DNA-targeting and sgRNA-targeting mechanisms, which were initially uncovered with dalbavancin and epirubicin and did not interfere with the loading of sgRNA or DNA substrates to Cas9 (Fig. 2C–F and Additional file 1: Fig. S4G-I), have not yet been fully uncovered with anti-CRISPR protein inhibitors [12]. On the other hand, additional mechanisms used for the anti-CRISPR protein, for example, AcrIIA5, which targets the active site of Cas9 [14], were not identified in our study, encouraging further inhibitor studies to enrich the pluripotency of small-molecule inhibitors. Epirubicin or dalbavancin seemed to show better potency than the previously identified BRD-series leads in the in vitro DNA-cleavage assay of *Spy*Cas9 or *Sau*Cas9 and in the *Spy*Cas9-based bacterial survival assay (Table 1, Fig. 4, Additional file 1: Fig. S3F-H, Fig. S7D-E and Fig. S14A-D), but the efficiencies of all four inhibitors (IC_{50} values ranging from 10 to 50 μM) (Fig. 5) were comparable to the reported value of BRD-series leads in mammalian cells [18, 19]. Mechanistically, pamoic acid or carbenoxolone could directly prevent the binding of DNA to Cas9 in the EMSA assays (Fig. 2C,D) and differ from the BRD-series leads, which do not directly compete with the substrate for binding to the PI domain at the PAM site [77]. Of note, pamoic acid and carbenoxolone, the substrate-competitive inhibitors, showed a 10–50 folds selectivity to the in vitro cleavage of the linear DNA substrate than that of the circular DNA substrate (Fig. 1B–E), indicating that the recognition between the DNA substrate and *Spy*Cas9 or *Sau*Cas9 is dependent on the topology of the DNA substrate. *Spy*Cas9 has been shown to more efficiently cleave
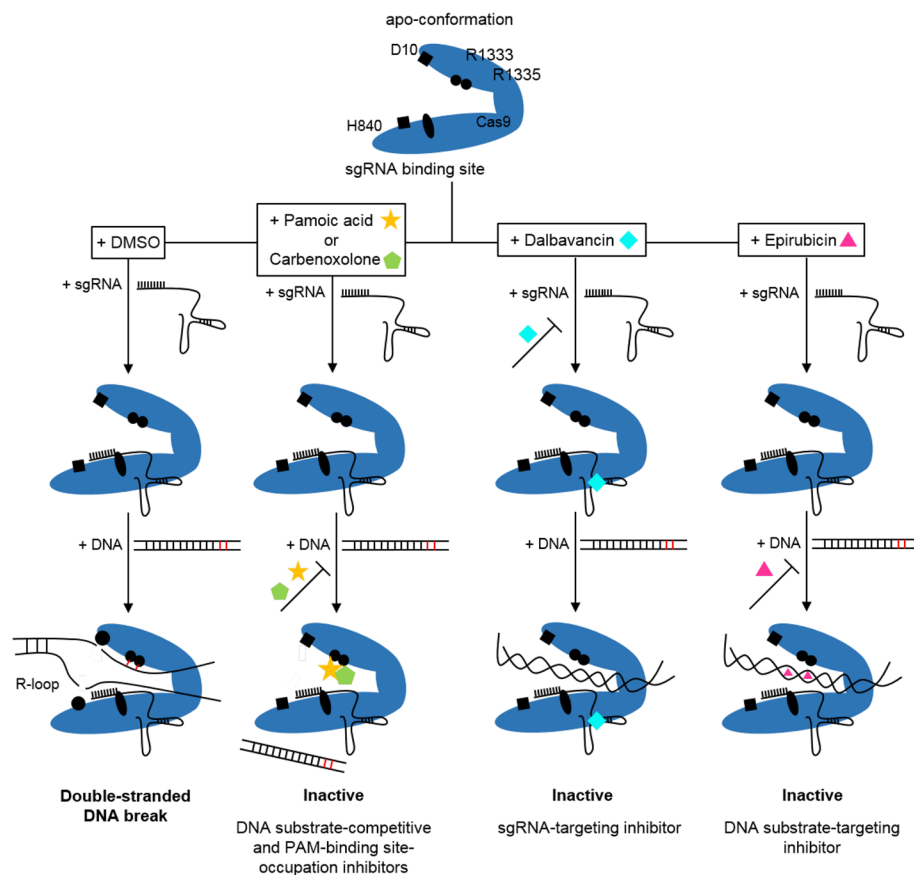
Fig. 7 Three proposed modes of action of four newly identified leads in inhibiting the activity of Cas9. Mode of action: pamoic acid or carbenoxolone binds competitively with DNA substrates to the PAM binding site of Cas9 positioned by Arg1333 and Arg1335, and shows a various inhibitory potency to the cleavage of the supercoil plasmid or linear DNA substrate by Cas9, and thus leading a selectivity on the cleavage of different topology of DNA. Dalbavancin directly binds to sgRNA and forms the quaternary complexes of Cas9 and sgRNA. Epirubicin directly binds to the DNA substrate and forms the quaternary complexes of Cas9 and DNA

the negative supercoil plasmid than linear DNA substrate as deduced from the sequence tolerance study on the N20 protospacer [78, 79], which resembles with our observations on the recognitions between the 5′-NGG, NAG or NGA PAM and the PI domain of Cas9 in the circular plasmid and linear DNA substrate (Figs. 1, 3B and Additional file 1: Fig. S6C). PAM tolerance gained by the negative supercoiling of DNA substrates was also recently observed for thermophilic Cas9 [80]. Collectively, these data imply that negative supercoiling facilitates not only the tolerance between N20 and sgRNA, but also that of PAM and the PI domain of Cas9, the latter of which may explain the selectivity of pamoic acid and carbenoxolone, the PAM-binding site-occupation inhibitors, between the cleavage of the supercoil plasmid and linear DNA (Fig. 7). The drastic difference, as probed by the potency of the small-molecule inhibitor of Cas9 (Table 1), quantitatively points out the prior hierarchy of DNA cleavage for Cas9, that is, supercoil DNA with an NGG PAM > supercoil DNA with an NGA or NAG PAM > linear DNA with an NGG PAM > linear DNA with an NGA or NAG PAM. Thus, the application of a Cas9 inhibitor to reduce the off-target effects must consider the topology of the target DNA in situ. Importantly, the substrate-competitive and PAM-binding site-occupation

mechanism, as represented by pamoic acid, could function in a *Spy*Cas9-mediated genome editing mouse model and was more efficient than the sgRNA-targeting mechanism (dalbavancin) (Fig. 6B and Additional file 1: Fig. S13F). Additionally, treatment of pamoic acid at doses ranging from 20 to 160 mg/kg could resist to the axing of Cas9, a dosage of which corresponds to the human-equivalent dose of ~ 1.6 to ~ 13 mg/kg when scaled with the interspecies body surface area (BSA) conversion method [81]. These dosages are reasonably achievable and frequently used in clinic, demonstrating a proof-of-concept for modulating the activity of Cas9 in vivo with small molecule inhibitors. Moreover, the chemical skeleton of pamoic acid, as well as other validated binders of Cas9 (Fig. 2A and Additional file 1: Fig. S4D), could offer several warheads for degrading Cas9 using proteolysis targeting chimera (PROTAC) technology [82].

For the substrate-targeting inhibitor epirubicin (Fig. 2D, F), an anthracycline-type inhibitor of eukaryotic TOP II, inhibitors of this type or the type of anthracenedione, a structural analog of epirubicin [83], but not other DNA-binding TOP II inhibitors with different mechanisms, inhibited the activity of *Spy*Cas9 (Additional file 1: Fig. S14E-F and Table S1). This finding indicates that epirubicin may specifically stabilize the complex of cleaved DNA and Cas9 at the minor groove of DNA in a unique manner similar to the inhibition of TOP II, i.e., selectively binding the base pairs at the -1 position flanking the double-strand break generated by TOP II, and non-covalently interacting not only with the DNA but also with TOP II, which has been verified by previous studies [84]. We constructed a putative 3D model for illustrating the interactions between epirubicin, the substrate DNA, and *Spy*Cas9 (Additional file 1: Fig. S14G). Nevertheless, the inhibitory mechanism of epirubicin on Cas9 remains largely unknown; however, it seems to serve as a tool for capturing the transition state of Cas9-DNA cleavage complex.

Although we have discovered a few DNA-topology-selective inhibitors for Type II-A Cas9, and uncovered the negative supercoiling of DNA could facilitate the PAM tolerance and the cleavage activity of Cas9 in the in vitro assays or in cells, the significances of these inhibitors or mechanisms in controlling the selectivity and activity of Cas9 to differential gene topologies need to be further explored at the genome level in cells and in vivo. Also, compared to the anti-CRISPR proteins that have been studied in detail for inhibitory mechanisms and utilized for various applications in vivo and in vitro [13, 16, 17], although the newly identified FDA-approved inhibitors except epirubicin display better bioavailability and rather safe profiles (Additional file 1: Fig. S15) [85–88], all these small-molecule inhibitors as well as BRD series inhibitors are still in their infancy and have to be extensively optimized in the drug R&D cycle before the application of them in genome-editing practices including but not limited to humans or clinics.

Hopefully, much knowledge on the elimination half-time ($t_{1/2}$ value) and drug metabolism has been accumulated for pamoic acid, carbenoxolone, epirubicin, and dalbavancin [85–89]. These inhibitors have respective $t_{1/2}$ values between 5.7 and 7.0 h, between 5.6 and 16.2 h, between 25 and 35 h, and of ~ 1 week in humans, and pamoic acid, carbenoxolone, and epirubicin are mainly metabolized in human liver while dalbavancin is largely eliminated in the kidney. In light of this valuable information, the application of these leads will be definitely accelerated.

Conclusions

In summary, we identified four FDA-approved drugs that could suppress the gene editing activity of *Spy*Cas9, *Sau*Cas9, and BE4 in an in vitro purified enzyme assay, in bacteria, mammalian cells, or mice via three distinct mechanisms. The DNA topology selectivity and PAM tolerance, as revealed by the substrate-competitive and PAM-binding site-occupation inhibitors of Cas9, offer valuable insights for efficient and precise editing of the gene in the context of 3D genome topology.

Methods

Plasmids and oligonucleotides

All plasmids and primers used in the cloning experiments and oligonucleotides are summarized in Additional file 1: Table S2 and S3, respectively. pET-28b-Cas9-His and p6 × His_NLS-SaCas9 were obtained from Addgene (Cambridge, MA) for the recombinant expression of *Spy*Cas9 (Addgene, #47,327) [90] and *Sau*Cas9 (Addgene, #101,086) [91] in *E. coli* (Additional file 1: Table S2). A series of plasmids with various mutations on *Spy*Cas9 (pET-28b-Cas9-D10A, pET-28b-Cas9-H840A, pET-28b-dCas9 or pET-28b-Cas9-VQR) (Additional file 1: Table S2) were constructed with site-directed mutagenesis method according to Strategene's instructions by using KOD-plus (TOYOBO, Osaka, Japan) and DpnI (New England Biolabs, NEB, Lincoln, NE), based on the pET-28b-Cas9-His template and the respective primer sets (No. 1–8, Additional file 1: Table S3).

The pcDNA3.1/CT-*GFP* plasmid used as a substrate for the in vitro cleavage assay was obtained from Thermo Fisher (#K482001, Waltham, MA), and a series of mutations on the 5′-NGG PAM site of the plasmid (5′-NAG, NGA and NAA PAM) (Additional file 1: Table S2-4) were accordingly made, based on pcDNA3.1/CT-*GFP* and the primers (No. 9–14, Additional file 1: Table S3). The non-target strand and target strand oligonucleotides (No. 16–19 and No. 81–82 for *Spy*Cas9; No. 26–27 for *Sau*Cas9), carrying the target sequence of *GFP* or *PCSK9* (Additional file 1: Table S4), were synthesized by Sangon Biotech (Shanghai, China) and labeled with a FAM fluorophore at the 5′ terminus of the non-target strand, before the annealing on Veriti 96-Well Thermal Cycler machine (Applied Biosystems, Waltham, MA) for making the double strands (ds) linear substrate for *Spy*Cas9 or *Sau*Cas9. Similarly, an 87-bp single-strand oligonucleotide (ssDNA; No. 20), carrying the same sequence of target-strand oligonucleotide (No. 17), was labeled with the 5′-FAM to monitor the cleavage activity of *Spy*Cas9 on ssDNA. The dual-labeled 5′-FAM 87 bp dsDNA (Additional file 1: Table S2) was obtained by annealing of the No. 16 and No. 20 oligonucleotides (Additional file 1: Table S3) to detect the activity of *Spy*Cas9 D10A or H840A nickase. The 2.5-kb linear dsDNA substrate with the 5′-NGG, NAG, or NGA PAM was obtained by amplifying the respective pcDNA3.1/CT-*GFP* template carrying various PAM (see above) with a primer set (No. 23–24).

For recombinant expression and purification of AcrIIA4, AcrIIA4 was amplified from the CMV-NLS-AcrIIA4 plasmid (Addgene #113,037) [17] and cloned into pET-28b using primers No. 21–22 (Additional file 1: Table S3).

The pCas (Addgene, #62,225) and pTargetF plasmids (Addgene, #62,226) were provided by Dr. S. Yang (CAS Center for Excellence in Molecular Plant Sciences, Chinese Academy of Sciences) [64]. The pTargetF (867 bp) plasmid (Additional file 1: Table S2) was obtained by inserting a synthesized oligonucleotide (Tsingke Biotechnology,

Additional file 1: Table S3, Beijing, China) carrying 493 bp X1 and 374 bp X2 homology directed repair (HDR) templates, which corresponded to 736 to 244 bp and -1 to -374 bp sequences of *SSEA* loci (NC_000913.3, 2,652494..2653339) [92], respectively, into an empty pTargetF vector. A 20-nucleotide encoding the spacer sequence of *Spy*Cas9 sgRNA (Additional file 1: Table S4) was then cloned into the pTargetF or pTargetF (867 bp) plasmid to generate the pTarget-sg*SSEA* or pTarget-sg*SSEA* (867 bp) plasmid using site-directed mutagenesis (No. 31–32, Additional file 1: Table S3). pCas-*Sau* (Additional file 1: Table S2) was constructed by replacing *Spy*Cas9 in the pCas plasmid with the *Sau*Cas9 insertion using the Seamless Assembly method (No. 33–36, Additional file 1: Table S3), which was generated by PCR-amplifying the *SauCas9* gene in p6 × His_NLS-SaCas9 (Additional file 1: Table S2). Similarly, pTarget-sg*SSEA* (867 bp)-*Sau* was constructed by cloning a pair of annealed oligonucleotides encoding a 21-bp spacer of sg*SSEA* (No. 37–38, Additional file 1: Table S3-4) at the SapI site in a plasmid, which was assembled with the PCR products from pX601 miniCMV-SaCas9 (Addgene, #107,055, Additional file 1: Table S2; a gift from Dr. Alex Hewitt, School of Medicine, University of Tasmania) and pTargetF (867 bp) by using Seamless Assembly (No. 39–42, Additional file 1: Table S3). To establish bacteria harboring these three plasmids, the pACYC184 plasmid (Addgene, #47,643) [93], with a p15A origin and chloramphenicol resistance, was selected to coordinate the RepA101 origin of pCas (kanamycin resistance, temperature-sensitive replication) and the pBR322 origin (spectinomycin resistance) of pTarget. pAC-AcrIIA4 was cloned into pACYC184 at KpnI and BamHI with No. 43–44 primers (Additional file 1: Table S3), and the respective control pAC-*GFP* plasmid was constructed using Seamless Assembly method using No. 45–48 primers, based on the pcDNA3.1/CT-*GFP* plasmid template and pACYC184 (Additional file 1: Table S2).

The annealed oligonucleotides were cloned into the all-in-one PX459 plasmid (Addgene, #107,055) to construct PX459-sg*COSMC* (No. 51–52, Additional file 1: Table S3), PX459-sg*EMX1* (No. 53–54), PX459-sg*GFP* (No. 55–56), or PX459-sg*PCSK9* (No. 83–84) using the recommended BbsI site [94]. The pGL3 plasmid (a generous gift from Dr. D. J. Pan, Soochow University) was mutated to pGL3-sg*EMX1* (No. 61–62) or pGL3-sg*GFP* (No. 67–68) by site-directed mutagenesis. pGL3-sg*COSMC-Sau* was obtained using Seamless Assembly and No. 63–66 primers containing an N21 protospacer for sg*COSMC* (Additional file 1: Table S3-4), based on the template of the scaffold sgRNA of the pX601 miniCMV-SaCas9 and the pGL3 empty vector (see above).

A pCDH-CMV-*GFP* plasmid, which contains the same protospacer and 5′-NGG PAM to the pcDNA3.1/CT-*GFP*, was constructed by cloning with the No. 69–70 primers and the pcDNA3.1/CT-*GFP* template (Additional file 1: Table S2-3). Then, the pCDH-CMV-*GFP* plasmid with a 5′-NAG PAM was generated by site-directed mutagenesis method with the No. 71–72 primers. pCDH-CMV-*COSMC* was generated by ligating a 350-bp PCR-amplified human *COSMC* gene into the pCDH-CMV empty vector [95] (No. 74–75, Additional file 1: Table S2-3).

The expression and purification of SpyCas9, SauCas9, and AcrIIA4

The 6 × His-tagged *Spy*Cas9 at the C-terminus was expressed in rosette (DE3) *E. coli* cells using pET-28b-Cas9-His (Addgene, #47,327), with the following modifications [90]. Briefly, 0.1 mM IPTG (Aladdin, I301904, Los Angeles, CA; final concentration) was

Zhang *et al. Genome Biology*   (2025) 26:75

Page 24 of 38

added into the culture for an overnight induction of the *Spy*Cas9 expression at 18 °C. The cells were collected by centrifugation and resuspended in $1 \times$ PBS before ultrasonication. After lysis, His-tagged *Spy*Cas9 was captured using a Ni–NTA affinity column (GE Healthcare, #17–5247-01, Chicago, IL) and eluted with Tris–HCl buffer (20 mM Tris, 500 mM imidazole, 500 mM NaCl, pH 7.5), according to the protocol described [90]. Next, the eluted fractions were further purified with a size exclusion Superdex™ 200 pg column (GE Healthcare, #28–9893-35) in the presence of 50 mM Tris–HCl buffer (150 mM NaCl, 5% glycerol (v:v), 2 mM DTT, pH 8.0), and the collected Cas9 peak was stored at -80 °C upon usage.

Similarly, $6 \times$ His-tagged *Spy*Cas9-D10A, *Spy*Cas9-H840A, dead *Spy*Cas9 with D10A and H840A mutations (dCas9), or *Spy*Cas9-VQR (D1135V/R1335Q/T1337R) mutant, as well as $6 \times$ His-tagged *Sau*Cas9 or AcrIIA4 (Additional file 1: Table S2), were expressed in rosette *E. coli* cells and affinity purified according to the procedures described above.

In vitro transcription of sgRNA

First, the spacer sequence of sgRNA (20 bp for *Spy*Cas9; 21 bp for *Sau*Cas9) targeting *GFP*, *COSMC*, and *PCSK9* was designed using the Eukaryotic Pathogen CRISPR guide RNA/DNA Design Tool (EuPaGDT) website (http://sgRNA.ctegd.uga.edu/) [96], whereas the sgRNAs for *SSEA* were retrieved using CRISPOR (http://crispor.tefor.net/) [97]. Second, the DNA template containing the sequences of the T7 RNA polymerase promoter, designed spacer, and scaffold of the respective sgRNA was synthesized by Sangon Biotech, that is No. 15 (for sg*GFP*), 25 (sg*GFP-Sau*), 30 (sg*SSEA*), 73 (sg*COSMC*), 80 (sg*PCSK9*), 89 (N20 spacer of sg*GFP*), 90 (scaffold of sg*GFP*), or 91 (epegRNA) oligonucleotides (Additional file 1: Table S3). Finally, the sgRNAs were in vitro transcribed with the GeneArt™ Precision sgRNA Synthesis Kit (Thermo Fisher; A29377) at 37 °C for 16 h and was then purified according to the manufacturer's instructions. The purified sgRNA was quantified with NanoDrop™ 2000c (Thermo Fisher) and then stored at -80 °C.

In vitro purified enzyme activity assays for Cas9

Assay setup and optimization

An enzyme assay to detect the endonuclease activity of purified *Spy*Cas9 was constructed and optimized based on a previously reported biochemical assay [1]. For the cleavage of circular plasmid substrates, His-tagged *Spy*Cas9 and in vitro transcribed sgRNA for *GFP* at an optimal concentration of 375 and 400 nM, respectively, were found to completely cleave 300 ng pcDNA3.1/CT-*GFP* plasmid in 20 mM HEPES buffer containing 150 mM KCl, 10 mM $MgCl_2$, 0.5 mM DTT, and 0.1 mM EDTA after an assay time of ~ 90 min (pH 7.5; Additional file 1: Fig. S1B). The assay tolerated a DMSO concentration of up to 2% in the presence of 0.01% Tween-20 (Additional file 1: Fig. S1C), a concentration commonly used to remove compound aggregates and avoid pan assay interference compounds (PAINS) [98, 99]. Typically, in a standard assay, 0.4 µl compound from the stock or their respective control DMSO (2%, final concentration) or ddH_2O was incubated with 18.6 µl HEPES buffer supplemented with 0.01% Tween-20 (the assay buffer, thereafter), which were from 15.6 µl HEPES buffer, 1 µl Tween-20 (0.2%), 1 µl purified *Spy*Cas9, and 1 µl respective sgRNA (375 and 400 nM for Cas9 and sgRNA, respectively), for 15 min before adding 1 µl pcDNA3.1/CT-*GFP* plasmid (300 ng) to start the assay in a 20 µl

volume. After a reaction time of 90 min at 37 °C, 5 µl 5 × loading buffer (250 mM EDTA, 1.2% SDS, and 30% glycerol [v:v] and bromophenol blue) was added to assay to terminate the reaction, and the products were electrophoresed on a 1% agarose gel with the TBE buffer (89 mM Tris, 89 mM boric acid, 2 mM EDTA, pH 8.0), stained with ethidium bromide (EB) and imaged under the Gel Image System (Tanon, Shanghai, China).

Primary inhibitor screening campaign

A compound collection composed of 1406 compounds of US Food and Drug Administration (FDA) or Foreign Approved Drugs (FAD)-approved drugs from Johns Hopkins Clinical Compound Library (JHCCL, Baltimore, Maryland), 2176 compounds from the Clinical Compound Library from TopScience Biotech Co. Ltd. (Shanghai, China), 109 compounds of the Approved Oncology Drugs Set or 118 natural products of the Natural Products Set from the National Cancer Institute (NCI; Bethesda, MD), and 798 natural products from TopScience Biotech Co. Ltd, were tested at 200 µM under the standard assay conditions (see above). Briefly, the enzyme assays for the primary inhibitor screening campaign were performed using GenexBeta multichannel 8 Channel Pipettes with equal tip spacing (Bio-DL, #11,087,439, Houston, TX) to add 0.4 µl compounds from the 10 mM stocks or 0.4 µl DMSO to the bottom of the wells in 8-strip tubes (Axygen, #0208-C, San Francisco, CA), followed by the addition of the assay buffer containing 375 nM *Spy*Cas9 and 400 nM anti-*GFP* sgRNA. After incubation for 15 min, 1 µl pcDNA3.1/CT-*GFP* was added to the assay buffer, and the enzyme assays were run and detected under standard conditions as described above. For each screening assay, a sample containing only 300 ng *GFP* plasmid was used as a control. The open circular and linear conformations of the plasmid in the EB-stained agarose gel were determined using the Fenton-reaction-mediated DNA damage assay and restriction endonuclease EcoRI (Additional file 1: Fig. S1B) [100, 101], respectively. Densitometry for the band of the linearized plasmid as well as the area containing the linear, open circular, and supercoil bands of the plasmid were quantified with ImageJ software (NIH, Bethesda, MD). The cleavage activity of Cas9 was calculated by dividing the band density of the linearized form by that of the total area and normalized to the DMSO group (100%). 228 compounds with less than 50% cleavage activity of *Spy*Cas9 in the primary screening were selected for secondary validation by testing them in duplicate at 200 µM and in a dose-dependent manner (Fig. 1A).

Dose-dependent tests of compounds for SpyCas9 or SauCas9

Compounds from the primary screening were tested for dose-dependent inhibition of the cleavage activity of Cas9 on the pcDNA3.1/CT-*GFP* plasmid (circular substrate, 300 ng) and/or the FAM-labeled 87 bp ds oligonucleotide (the linear substrate with the same protospacer and PAM as the *GFP* plasmid, 10 nM) (Additional file 1: Table S2-4) under standard assay conditions (for the assay optimization under the 87-bp linear substrate; see Additional file 1: Fig. S1D). A total of 31 compounds were found to have IC_{50} values less than 200 µM in inhibiting the cleavage of either *GFP* plasmid or oligonucleotide substrate (Fig. 1A and Additional file 1: Fig. S2). Moreover, the same substrate concentrations, that is, 10 nM for the linear substrate or 300 ng for the circular plasmid, were used under the standard assay conditions for detecting the effect of compounds on the

cleavage of *GFP* plasmids with the 5′-NAG or NGA PAM (Fig. 3B and Additional file 1: Fig. S6D), 2.5 kb linear *GFP* dsDNA with the 5′-NGG, NAG, NGA, or NAA PAM (Additional file 1: Fig. S3C and S7A), dual-labeled 5′-FAM 87 bp *GFP* dsDNA (Fig. 3C) or 5′-FAM 87 bp *GFP* ssDNA (Fig. 2H), and on the cleavage of *SSEA* plasmid (Additional file 1: Fig. S7B) or *COSMC* plasmid (Additional file 1: Fig. S9C) as well as on the cleavage of 5′-FAM 77-bp *PCSK9* dsDNA (Additional file 1: Fig. S13A). For the activity assay of *Sau*Cas9, 100 nM purified *Sau*Cas9 and 100 nM sgRNA in the presence of 300 ng *GFP* plasmid or 10 nM 5′-FAM 87 bp ds oligonucleotide with a 5′-TTGAAT PAM (Fig. 1D-E and Additional file 1: Table S4) were used in the standard assays.

To detect the cleaved product from the plasmid or 2.5 kb dsDNA substrate, a 1% agarose gel was used, and the product was stained with EB and quantified accordingly (see above). To detect the cleavage of the FAM-labeled oligonucleotide, a 20% polyacrylamide native gel (Fig. 1C, E, or 2H) or a 12% denatured polyacrylamide gel containing 8 M urea (Fig. 3C) was used to separate the cleaved products, and the fluorescent signals of the FAM-labeled substrate and products were recorded under excitation at 488 nm on a ChemiDoc scanner (Bio-Rad, Hercules, CA). The cleavage activity of Cas9 was calculated by dividing the band density of the product by the total area and normalizing to the DMSO group (100%).

The activity assays for NEB Cas9, SpRY-Cas9, FnoCas12a, or LbaCas12a

For the detection of the effects of inhibitors on the commercially available *Spy*Cas9 (NEB, M0386T), SpRY-Cas9 (NEB, M0669T), *Fno*Cas12a, or *Lba*Cas12a enzymes (Tolo-Bio, #32,106–03 or #32,108–03, Shanghai, China), the latter two of which are a Type V CRISPR/Cas proteins [63], we incubated the inhibitors with 100 nM ribonucleoprotein of *Spy*Cas9 and sgRNA, with 150 nM ribonucleoprotein of SpRY-Cas9 and sgRNA, 50 nM *Fno*Cas12a or 50 nM *Lba*Cas12a in the NEBuffer™ r3.1 (NEB, B6003V), and 1 × HOLMES Buffer 1 (ToloBio, 32,106–03), respectively, as recommended by the supplies. After an incubation of 15 min, 300 ng *GFP* plasmid, 10 nM 5′-FAM 87 bp ds oligonucleotide, or 50 nM pre-mix of crRNA: target DNA (10:1, ToloBio; target DNA: 825 bp DNA methyltransferase 1 fragment) was added to the respective assay, and the cleaved DNA was detected accordingly.

Surface plasmon resonance assays

A 100 μg/ml *Spy*Cas9 was immobilized onto the surface of the CM5 sensor chip using an amino-coupling kit, and the inhibitors were then tested using surface plasmon resonance assays (SPR) on a Biacore™ 8 K (GE Healthcare). The inhibitors were diluted with 1 × PBST to the indicated concentrations before being loaded onto the sensors, and the response curve was recorded at a flow rate of 30 μl/min flow rate, binding process time of 120 s, and dissociation time of 120 s. The equilibrium affinity constant (K_D) values were calculated using BIAcore evaluation software (version 3.1).

Electrophoretic mobility shift assay

An electrophoretic mobility shift assay (EMSA) was employed to assess the effect of the inhibitors on the binding of the substrate DNA to *Spy*Cas9 (Fig. 2C,D) or on the binding of sgRNA to the enzyme (Fig. 2E) accordingly [102]. For the binding of DNA,

dCas9-sgRNA (100 nM: 400 nM; Fig. 2C) binary complex or dCas9 (100 nM; Fig. 2D) was sequentially incubated with the DNA substrate (10 nM 5′-FAM labeled 87 bp *GFP* ds oligonucleotide, 300 ng the *GFP* plasmid or 25 nM ds oligonucleotides containing 8 × PAM (No. 28–29 in Additional file 1: Table S3)) for 15 min and then inhibitors for 15 min at room temperature (RT), or with a reverse order of inhibitors and then substrate, in the EMSA binding buffer (20 mM Tris, 20 mM KCl, 5 mM EDTA, 1 mM DTT, 5% glycerol, 50 µg/ml heparin, 0.01% Tween-20, 100 µg/ml BSA; pH 7.5). Then, the complex composed of the inhibitor, dCas9 protein, or sgRNA was mobilized on a 6% native poly-acrylamide gel for the oligonucleotide or on a 1% native agarose gel for the *GFP* plasmid before the visualization with $1 \times SYBR^{™}$ Gold (Thermal Fisher, S-11494, Wilmington, MA; Fig. 2C, right panel; Fig. 2D, right panel) and the imaging for the fluorescence of FAM at 488 nm under an excitation of 488 nm (Fig. 2C, left and upper panels; Fig. 2D, left panel) or dying with EB (Fig. 2C, bottom panels). Similarly, for sgRNA binding, the compounds were incubated with 400 nM sgRNA or dCas9: sgRNA (100 nM: 400 nM) for 15 min in the presence or the absence of 50% (w/v) formamide, a regent that disrupts the secondary structure of sgRNA, before separation on a 6% polyacrylamide gel or a 12% polyacrylamide gel containing 8 M urea and staining with $1 \times SYBR$ Gold (Fig. 2E and Additional file 1: Fig. S5A-B).

Thermal shift assay

Thermal shift assays were performed in 96-well PCR plates using the LightCycler 96 RT-PCR Instrument (Roche, Penzberg, Germany) [18]. A 1 µM *Spy*Cas9: sgRNA complex (1:1) was diluted in the thermal shift assay buffer (20 mM Tris–HCl, 150 mM NaCl, 10 mM EDTA, 5 mM DTT, pH 7.5) and incubated with annealed ds oligonucleotides containing 8 × PAM at a molar ratio of 0.5:1, 1:1, 2:1, or 5:1 (substrate: Cas9) in the presence or absence of inhibitor in a total volume of 10 µL. After 15 min incubation at RT, $1 \times SYPRO^{™}$ Orange dye (Thermal Fisher, S-6650) was added and the emission fluorescence of 570 nm under an excitation of 470 nm was then recorded along the temperature change from 25 to 95 °C at a rate of 0.5 °C per second in the RT-PCR Instrument. The unfolding transition midpoint temperature (Tm) of *Spy*Cas9 was obtained by fitting the sigmoidal curves to the Boltzmann equation using GraphPad software (version 8.4, San Diego, CA).

Molecular modeling

To construct the binding model of pamoic acid or carbenoxolone to *Spy*Cas9, the substrate-competitive inhibitors, co-crystal structures of *Spy*Cas9, AcrIIA4, and sgRNA (PDB code: 5VW1) [16], and of *Spy*Cas9, dsDNA, and sgRNA (PDB code 4UN3) [4] were analyzed. The structures of pamoic acid and carbenoxolone were manually drawn according to the coordinates of the 3D structure of the Asp69-Glu70 dipeptide in AcrIIA4 (Fig. 3D and Additional file 1: Fig. S6A) using Discovery Studio software (version 3.5; Accelrys, San Diego, CA). The structures of the compounds were optimized via a 2000 step minimization using Discovery Studio.

For epirubicin, the co-crystal structures of human TOP II, DNA, and amsacrine (PDB code: 4G0U) [103], an analog of epirubicin and a known inhibitor of human TOP II [27, 103], were obtained, and the structure of amsacrine was replaced with that of epirubicin according to the coordinates of amsacrine. The DNA and epirubicin complex was extracted and optimized via a 2000 step minimization before being superimposed onto the DNA structure in the crystal structures of *Spy*Cas9, DNA, and sgRNA (PDB code: 7S4X) [104].

Bacterial assays for detecting the activity of SpyCas9 and SauCas9

Two-plasmid-based bacterial survival assay

A previously developed two-plasmid-based genome editing method for bacteria [64], was adopted to monitor the activity of *Spy*Cas9 or *Sau*Cas9 in the absence (Fig. 4A,B) or presence of a homologous recombination repair template (Fig. 4C,D) in MG1655 bacteria. Briefly, MG1655 competent cells expressing *Spy*Cas9 or *Sau*Cas9 (pCas-competent cells) were prepared using pCas (#62,225; Addgene) or pCas9-*Sau* (Additional file 1: Table S2) in the presence of 20 mM L-arabinose. Next, 300 ng of pTargetF (Addgene, #62,226) or pTarget-sg*SSEA* (Additional file 1: Table S2) was electroporated into the pCas competent cells in a 0.1-cm Gene Pulser®/MicroPulser™ Electroporation Cuvette (Bio-Rad, #1,652,089) with Gene Pulser Xcell™ Electroporation System (Bio-Rad, #165–2660) under conditions of 1800 V and 5.2 ms. Immediately after the electroporation, the compounds were added into 700 μl LB of the bacteria and incubated for 1.5 h at 32 °C, which were subcultured at 32 °C in LB agar plates containing 100 μg/ml kanamycin (Sangon, A506636) and 100 μg/ml spectinomycin (Sangon, A600901) for the selection of viable bacteria colonies. After overnight culture, the agar plate was photographed using the Gel Image System, and the colony number in the agar plates was counted using the Colony Counter software (version 3.2, Tanon). The DNA of the *SSEA* loci from the colonies was sequenced using Sanger sequencing and found to be wt *SSEA*.

PCR-based genotyping assay

Next, 300 ng of pTarget-sg*SSEA* (867 bp) or pTarget-sg*SSEA* (867 bp)-*Sau* (Additional file 1: Table S2) carrying an 867-bp homologous recombination repair template (Additional file 1: Table S3) was electroporated into the pCas competent cells under the same conditions (see above). Next, compounds were added into the 1 ml LB suspension of the bacteria containing 200 μg/ml kanamycin and 200 μg/ml spectinomycin and incubated at 32 °C for 20 h. Then, 2 μl aliquots were taken to conduct colony PCR with the primer No.49–50 and $2 \times$ Hieff™ PCR Master Mix (Yeasen Biotech, #10102ES03, Shanghai, China). The PCR products (1152 bp for unedited wt *SSEA*, 909-bp for *Spy*Cas9-edited or *Sau*Cas9-edited strains) were then separated on a 1% agarose gel, and the editing efficiency was calculated as the ratio between the band density of the 909-bp gene type and the sum of the 909 bp and 1152 bp gene types. To test the effect of AcrIIA4, competent cells harboring both pCas and pAC-AcrIIA4 plasmids (Additional file 1: Table S2) were prepared in the presence of 20 mM L-arabinose and 0.5 mM IPTG. Then, the cells were electroporated with pTarget-sg*SSEA* (867 bp) and genotyped for the *SSEA* according to

the procedures described above. The sequences of the PCR products were verified by Sanger sequencing to correspond to the sizes of the PCR bands.

Cell culture and stable cell line

HEK293FT cells were a kind gift from Dr. W.L. Jin (Lanzhou University, Gansu, China), and HEK293T was a gift from Dr. H. Gehring (University of Zurich, Zurich, Switzerland), whereas HT29 cells were originally obtained from the Shanghai Cell Bank (Chinese Academy of Science, Shanghai, China). HEK293FT, HEK293T, and HT29 cells were maintained in DMEM (Gibco, Grand Island, NY) supplied with 10% heat-inactivated fetal bovine serum (Lonsera, Los Angeles, CA) and 1% penicillin/streptomycin (Biosharp, Guangzhou, China), in a humidified 5% CO_2 atmosphere at 37 ℃.

HEK293FT cells stably expressing GFP were constructed using lentiviral particles carrying pCDH-CMV-*GFP* (Additional file 1: Table S2) and pPACK Packaging Plasmid Mix (SBI, Mountain View, CA) according to the manufacturer's instructions. The stable cells were accordingly cultured in the DMEM containing 2.5 µg/ml puromycin (Cayman, #13,884, Ann Arbor, MI).

The cell lines were not authenticated after obtaining but routinely checked to be free of mycoplasma contamination.

Comet assay

The genotoxicity of the Cas9 inhibitors was evaluated by using a comet assay kit (Beyotime, Shanghai, China) according to the manufacturer's protocol [105]. Briefly, HEK293T cells were seeded at a density of 1×10^5 cells/well in a 12-well plate and treated with epirubicin, H_2O_2, pamoic acid, dalbavancin, or carbenoxolone at the indicated concentrations for 4 or 24 h. Then, the cells were harvested and the density of the suspension was adjusted to 1×10^6 cells/ml with ice-cold PBS. The cell samples (10 µL) were subsequently mixed with 75 µL low melting agarose before being placed on a glass slide, which was precoated with 1% normal melting agarose. The slides were solidified at 4 ℃ and the cells were lysed with a cold lysis buffer at 4 ℃ for 1 h. Then, the slides were soaked in alkaline electrophoresis solution (200 mM NaOH, 1 mM EDTA, pH 13) for 30 min to unwind the DNA, and the electrophoresis was performed at 200 mA for 30 min. Subsequently, the slide was fixed with ethanol before staining with propidium iodide. Imaging was performed using a confocal laser scanning fluorescence microscopy (A1Si, Nikon, Tokyo, Japan). The quantitation of TailDNA was quantified in at least 20 cells per group with CASPLab software (version 1.2.3, beta2).

Cell viability

HEK293FT or HT29 cells were seeded at $\sim 2 \times 10^4$ cells per well in a 96-well plate (Corning, #353,227, Corning, NY) for a day; 0.4 µL DMSO (0.4%, final concentration) or inhibitors at different concentrations were added to the 100 µl culture and incubated with the cells overnight. Then, the cells were assayed for determination of the cell viability using the CellTiter 96® Aqueous One Solution Cell Proliferation Assay (Promega, G3581, Madison, WI) according to the standard protocols.

LDH-based cell toxicity assay

To determine the cytotoxicity of the Cas9 inhibitors, a CytoTox-ONE Homogeneous Membrane Integrity Assay (Promega) was used according to the manufacturers' instructions. Briefly, HEK293T or HT29 cells were seeded at a density of 6000 cells/well in a 96-well plate before the treatment with pamoic acid, carbenoxolone, or dalbavancin at the indicated concentrations for 24 h. For a positive control, the cells were treated with 2 µL lysis buffer (9% Triton X-100, w/v). Then, the medium (50 µL) was transferred to a Nunc MaxiSorp black 96-well plate and mixed with CytoTox-ONE reagent (50 µL). After a 10-min incubation at 22 °C, 50 µl of stop solution was added and the activity of LDH was calculated by measuring the fluorescence emission at a wavelength of 590 nm under an excitation of 560 nm on a microplate reader.

GFP disruption assay

HEK293FT wt cells or HEK293FT cells stably expressing GFP were seeded at a volume of 1 ml with $\sim 2 \times 10^5$ cells per well in 12-well plates for 1 day, and 1 µg of PX459-*Spy*Cas9 (Addgene, #62,988) together with 1 µg of pGL3-sg*GFP* or empty vector (Additional file 1: Table S2) were then transiently transfected into the cells using Lipofectamine™ 3000 transfection reagent according to the manufacturer's protocol (Thermal Fisher, L3000008). Immediately after transfection, the inhibitors or their respective controls (DMSO or ddH$_2$O) were added and incubated with the cells for 24 h. The treated cells were further cultured in the presence of 2.5 µg/ml puromycin for additional 36–48 h before collecting for the analysis of flow cytometry.

Similarly, for the disruption assay of plasmids, HEK293FT wt cells were seeded and transiently transfected with 1 µg pCDH-*GFP* plasmid with a 5′-NGG or NAG PAM together with 1 µg PX459-*Spy*Cas9-sg*GFP* or PX459-*Spy*Cas9-sg*Control* (Additional file 1: Table S2). Six hours post transfection, the cells were treated with the compound for 24 h, colonies were selected with puromycin, and the remaining cells were analyzed by flow cytometry as described above.

Flow cytometry

After trypsinization, the cells were washed and resuspended with 400 µl of $1 \times$ PBS and the expression of GFP was analyzed by detection of the GFP fluorescence with a LSR Fortessa flow cytometer (BD Bioscience, Franklin Lake, NJ). The data were recorded at 500/50 nm (green fluorescence) wavelength after excitation at 488 nm. For each sample, at least 10,000 cells were analyzed. Data were analyzed using FlowJo software (version 7.6, San Francisco, CA).

Genome editing by SpyCas9, SauCas9, or BE4 at the endogenous COMSC or EMX1 site

SpyCas9 or SauCas9-mediated genome editing in HEK293FT cells

For *Spy*Cas9-mediated genome editing, HEK293FT or HT29 wt cells were seeded at $\sim 2 \times 10^5$ cells per well in 12-well plates for 1 day, and 1 µg PX459-*Spy*Cas9-sg*COSMC* or PX459-*Spy*Cas9-sg*EMX1* as well as PX459-*Spy*Cas9-sg*Control* were transfected into cells with Lipofectamine™ 3000 transfection reagent for 1 day. Subsequently, the compounds were added to the culture at 0 or 6 h post the transfection, and the cells were cultured at 37 °C for additional 24 h, before the selection with the 2.5 µg/ml puromycin

for 36–48 h. Next, the target DNA at the *COSMC* or *EMX1* loci in the cells was analyzed by Sanger sequencing or next-generation sequencing. To assess the inhibitory effect of AcrIIA4, a known protein inhibitor of *Spy*Cas9, HEK293FT cells were co-transfected with the PX459-*Spy*Cas9 plasmid containing sg*COSMC*, sg*EMX1*, or sg*Control* with the CMV-NLS-AcrIIA4 plasmid (Addgene, #113,037) using Lipofectamine™ 3000 before standard treatment and analysis as described above.

For *Sau*Cas9-mediated genome editing, 1 μg miniCMV-SaCas9 plasmid (Addgene, #107,055) coding *Sau*Cas9 together with 1 μg pGL3 containing sg*COSMC-Sau* or sg*Control* were co-transfected into HEK293FT wt cells using Lipofectamine™ 3000 according to the manufacturer's protocol. Immediately after transfection, the inhibitors were added and incubated for 24 h before colony selection with 2.5 μg/ml puromycin and target DNA analysis with Sanger sequencing, which were sequentially performed under a same protocol as described above.

BE4-mediated base editing in HEK293FT cells

A 1 μg pCMV-AncBE4max and 1 μg of pGL3 plasmid, encoding a respective BE4 system, and sg*EMX1* or sg*Control* [71] were co-transfected into HEK293FT wt cells using Lipofectamine™ 3000 accordingly. Transfected cells were simultaneously incubated with the inhibitors for 24 h before selection and Sanger sequencing.

Analysis for the efficiency of Cas9 or BE4 -mediated genome editing

Genomic DNA from puromycin-selected colonies was extracted using a Blood/Cell/Tissue Genomic DNA Extraction Kit (Tiangen, DP304-03, Beijing, China), according to the manufacturer's instructions. Next, the ~ 450–550 bp target DNA of *COSMC* or *EMX1* containing the sgRNA and PAM sites was amplified from the 100 ng genome DNA with the corresponding primers (No. 57–58 for *COSMC*, No. 59–60 for *EMX1*) (Additional file 1: Table S3), using $2 \times$ Hieff™ PCR Master Mix under a PCR condition of pre-heat at 98 °C for 4 min, 40 cycles of amplification (98 °C for 40 s, 60 °C for 30 s, 72 °C for 40 s) and final extension at 72 °C for 10 min. After a purity check on 1% agarose gels, the PCR products were sent for Sanger sequencing, performed by Sangon Biotech.

To quantify the editing efficiency of *Spy*Cas9 or *Sau*Cas9 at the *COSMC* or *EMX1*site in HEK293FT cells, sequencing chromatograms from Sanger sequencing were analyzed using the Tracking of Indels by Decomposition (TIDE) website (https://tide.nki.nl/) [66]. To analyze the base editing efficiency, Sanger sequencing data of *EMX1* from BE4 base-editor-treated HEK293FT cells were submitted to a program named Edit Deconvolution by Inference Of Traces In R (EditR (https://moriaritylab.shinyapps.io/editr_v10/) [66, 67]. The C-to-T conversion efficiencies at the C_5 or C_6 positions of the *EMX1* site were analyzed accordingly.

T7EI assay

A total of ~ 800 ng purified PCR product (see above) was annealed under conditions of 95 °C for 5 min, ramp down to 85 °C with 2 °C/s, ramp down to 25 °C at 0.1 °C/s, and final holding at 4 °C for 5 min, before an incubation with 1 μl (10 U, final) of T7 Endonuclease I enzyme (T7EI, Genscript Biotech, Z03396, Nanjing, China) at 37 °C for 15 min. Enzymatic products were purified using a PCR clean-up kit (Macherey–Nagel,

Germany), electrophoresed on a 2% agarose gel, and stained with EB. The DNA bands of the substrate (input) and products (T7 fragments) were quantified with ImageJ software, and the percentage of Indels was calculated by dividing the band density of the products by that of the total input [68].

Western blot

After the treatment with inhibitors and puromycin, the transfected HEK293FT cells were collected and lysed in $1 \times$ PBS containing 1% Nonidet P40 (Applichem, Berlin, Germany) and 1 mM PMSF (Sangon, Shanghai, China) for 2 h at 4 °C. After centrifugation, the supernatant was extracted and the total protein amount was quantified using a Pierce™ BCA Protein Assay Kit (Thermo Fisher, #23,225) according to the manufacturer's instructions. Equal amount of the extracted protein from supernatant was loaded and separated in a 10% SDS-PAGE before transferred on to a PVDF membrane and blotting for Flag-tagged Cas9 and β-actin with the anti-Flag (Abmart, M20008M, Shanghai, China) and anti β-actin antibody (Abmart, M20011S), respectively. The optical densities of the Cas9 and β-actin protein bands were quantified using ImageJ software and are shown as ratios below the gel.

RT-PCR analysis

After treatment with the inhibitors for 24 h, total mRNAs from the transfected HEK293FT cells were isolated using RNAiso Plus (#9109; TaKaRa, Kyoto, Japan) according to the manufacturer's instructions. Then, the cDNA was reverse-transcribed using oligo-dT with the Eastep® RT Master Mix (Promega, LS2050). A 2 μl of cDNA was used for Real-time PCRs to measure the mRNA levels of *Cas9* or *GAPDH* using Hieff® qPCR SYBR Green Master Mix (Yeasen Biotech, #11204ES03) and LightCycler 96 RT-PCR Instrument (Roche) with the specific primer (No. 76–77 for *Cas9*, No. 78–79 for *GAPDH*; Additional file 1: Table S3). Gene expression quantification was completed by normalization to *GAPDH* using the $\Delta\Delta^{ct}$ method [106].

Administration of drugs and hydrodynamic injection in mice

Mice

BALB/c mice (7 weeks in age, 22–25 g body weight, male) for the construction of an anti-*PCSK9* mice model with hydrodynamic injections of an all-in-one Cas9-sgRNA plasmid were purchased from Shanghai SLAC Experimental Animal (Shanghai, China). The animals were maintained on a daily 12 h light/dark cycle and fed a normal chow diet at RT. All experiments were approved by the Institutional Animal Care and Use Committee (IACUC) of Shanghai Jiao Tong University, China.

Administration of drugs

BALB/c mice were intraperitoneally injected three times with the inhibitors at doses of 10, 20, 40, 80, or 160 mg/kg, or saline on days 0, 3, and 6 in a mouse study with three treatment cycles of 3 days, as outlined in Fig. 6A. To determine the basal effect of the inhibitor alone on PCSK9 levels, 160 mg/kg pamoic acid, dalbavancin, carbenoxolone, or saline was administered thrice to the mice, followed by three hydrodynamic injections of PX459-*Spy*Cas9-sg*Control* on days 1, 4, and 7 (Additional file 1: Fig. S13C). Similarly,

10, 20, 40, 80, or 160 mg/kg pamoic acid, dalbavancin, or carbenoxolone as well as saline was administered to the PX459-*Spy*Cas9-sg*PCSK9*-treated mice (Fig. 6B).

Hydrodynamic injection

To construct a *Spy*Cas9-mediated anti-*PCSK9* mouse model, BALB/c wt mice were hydrodynamically injected with 2 ml saline containing 90 µg all-in-one PX459-*Spy*Cas9-sg*PCSK9* plasmid or PX459-*Spy*Cas9-sg*Control* in the tail vein for 5–8 s on days 1, 4, and 7, according to a protocol described previously [107]. Approximately 100 µl blood sample from the orbital sinus was collected through capillaries on days 2, 5, and 8 for analysis of the plasma amount of PCSK9 (Additional file 1: Fig. S13B). To test the effect of inhibitors, the PX459-*Spy*Cas9-sg*PCSK9* plasmid or PX459-*Spy*Cas9-sg*Control* was delivered to saline- or inhibitor-pre-treated mice (Fig. 6B or Additional file 1: Fig. S13C), and the corresponding blood was collected for further analysis. The mice underwent three treatment cycles of the compounds and were sacrificed on day 8, and the liver tissues were collected for Indel analysis of *PCSK9* locus with next-generation sequencing (NGS) analysis.

PCSK9 ELISA

Blood samples from mice were collected in 1.5-ml heparin-coated Eppendorf tubes. After a centrifugation at 4000 rpm for 10 min at 4 °C, the plasma samples were obtained and stored at -80 °C. Twenty microliters of plasma was used to determine the amount of PCSK9 using a mouse proprotein convertase 9/*PCSK9* Quantikine ELISA kit according to the standard protocol provided by the manufacturer (R&D, MPC900, Minneapolis, MN).

Total cholesterol

A total of 2.5 µl of plasma was used to quantify total cholesterol using a total cholesterol detection kit (NJJCBIO, A111-1–1, Nanjing, China) according to the manufacturer's protocol.

Next-generation sequencing

Approximately 10 mg of liver tissue was ground in $1 \times$ PBS, and a cell suspension was obtained via filtration using a 400-mesh gauze. Genomic DNA was extracted from the isolated liver cells using the Blood/Cell/Tissue Genomic DNA Extraction Kit and was used to amplify the target DNA from the *PCSK9* site with primer No. 85–86 (Additional file 1: Table S3). The editing efficiency and genotype in the *PCSK9* locus of mouse liver were accordingly analyzed using NGS. For the NGS, 100 ng genomic DNA was used as a DNA template and was amplified by PCR with the primer set containing sequences complementary to Illumina P5/P7 adapters (No. 87–88, Additional file 1: Table S3) under a condition of pre-heat at 98 °C for 5 min, 40 cycles of amplification (98 °C for 40 s, 60 °C for 30 s, 68 °C for 30 s) and final extension at 68 °C for 10 min. The resulting PCR product of *PCSK9* was purified using a PCR clean-up kit and was further amplified with commercial P7 and P5 primers before sequencing in paired-end mode with a read length of 150-bp and $\sim 7000 \times$ depth per nucleotide on an Illumina MiSeq PE150

Zhang *et al. Genome Biology*   (2025) 26:75

Page 34 of 38

machine (Illumina, San Diego, CA) provided by Tsingke Biotechnology. The percentage of reads modified was determined by the sequencing data using CRISPResso2 [108].

Similarly, the NGS was performed for the samples from the HEK293FT cells with the primer set (No. 92–93, Additional file 1: Table S3) targeting the *COSMC* site and the percentage of reads modified was accordingly analyzed.

Statistical analysis

Dose-dependent curves were generated by fitting the raw data with nonlinear regression and sigmoidal dose–response curves using GraphPad (version 8.4, San Diego, CA). Statistical analysis was performed on the raw data for each group using Student's t test, two-way ANOVA with Bonferroni post-tests, one-way ANOVA with Tukey's multiple comparison tests, or Dunnett's multiple comparison tests using GraphPad.

Supplementary Information

The online version contains supplementary material available at https://doi.org/10.1186/s13059-025-03521-w.

> Additional file 1. Supplementary Table S1-S4 and figures S1-S15.

Peer review information
Shuangxia Jin and Andrew Cosgrove were the primary editors of this article and managed its editorial process and peer review in collaboration with the rest of the editorial team. The peer-review history is available in the online version of this article.

Authors' contributions
Y.X.Z. and F.W. designed the study and analyzed the data. Y.X.Z. constructed the purified enzyme, bacterial, mammalian cell and mice assays. W.T.Z., Y.X.Z., Y.Y.Z. and J.Q.C. constructed the in vitro purified enzyme assay, performed the low-throughput screening and quantified the screening data. Y.T.H. constructed the docking models of inhibitor and Cas9. Y.X.Z. and F.W. wrote the paper. All authors reviewed the results and approved the final version of the manuscript.

Data availability
 The raw sequencing data have been deposited to the NCBI SRA under accession number PRJNA1224298.

Declarations

Ethics approval and consent to participate
The animal study was approved by the Institutional Animal Care and Use Committee (IACUC) of Shanghai Jiao Tong University, China.

Consent for publication
Not applicable.

Competing interests
The authors declare no competing interests.

Zhang *et al. Genome Biology*   (2025) 26:75

Page 35 of 38

References

1. Jinek M, Chylinski K, Fonfara I, Hauer M, Doudna JA, Charpentier E. A programmable dual-RNA-guided DNA endonuclease in adaptive bacterial immunity. Science. 2012;337:816–21.
2. Cong L, Ran FA, Cox D, Lin S, Barretto R, Habib N, Hsu PD, Wu X, Jiang W, Marraffini LA, et al. Multiplex genome engineering using CRISPR/Cas systems. Science. 2013;339:819–23.
3. Nishimasu H, Ran FA, Hsu PD, Konermann S, Shehata SI, Dohmae N, Ishitani R, Zhang F, Nureki O. Crystal structure of Cas9 in complex with guide RNA and target DNA. Cell. 2014;156:935–49.
4. Anders C, Niewoehner O, Duerst A, Jinek M. Structural basis of PAM-dependent target DNA recognition by the Cas9 endonuclease. Nature. 2014;513:569–73.
5. Jinek M, Jiang F, Taylor DW, Sternberg SH, Kaya E, Ma E, Anders C, Hauer M, Zhou K, Lin S, et al. Structures of Cas9 endonucleases reveal RNA-mediated conformational activation. Science. 2014;343:1247997.
6. Leenay RT, Beisel CL. Deciphering, communicating, and engineering the CRISPR PAM. J Mol Biol. 2017;429:177–91.
7. Enache OM, Rendo V, Abdusamad M, Lam D, Davison D, Pal S, Currimjee N, Hess J, Pantel S, Nag A, et al. Cas9 activates the p53 pathway and selects for p53-inactivating mutations. Nat Genet. 2020;52:662–8.
8. Cullot G, Boutin J, Toutain J, Prat F, Pennamen P, Rooryck C, Teichmann M, Rousseau E, Lamrissi-Garcia I, Guyonnet-Duperat V, et al. CRISPR-Cas9 genome editing induces megabase-scale chromosomal truncations. Nat Commun. 2019;10:1136.
9. Zhang XH, Tee LY, Wang XG, Huang QS, Yang SH. Off-target effects in CRISPR/Cas9-mediated genome engineering. Mol Ther Nucleic Acids. 2015;4:e264.
10. Fu Y, Foden JA, Khayter C, Maeder ML, Reyon D, Joung JK, Sander JD. High-frequency off-target mutagenesis induced by CRISPR-Cas nucleases in human cells. Nat Biotechnol. 2013;31:822–6.
11. Kimberland ML, Hou W, Alfonso-Pecchio A, Wilson S, Rao Y, Zhang S, Lu Q. Strategies for controlling CRISPR/Cas9 off-target effects and biological variations in mammalian genome editing experiments. J Biotechnol. 2018;284:91–101.
12. Hwang S, Maxwell KL. Diverse mechanisms of CRISPR-Cas9 inhibition by type II anti-CRISPR proteins. J Mol Biol. 2023;435:168041.
13. Dong GM, Wang S, Zhu Y, Wang S, Xiong Z, Yang J, Xu Z, Huang Z. Structural basis of CRISPR-SpyCas9 inhibition by an anti-CRISPR protein. Nature. 2017;546:436–9.
14. Song G, Zhang F, Zhang X, Gao X, Zhu X, Fan D, Tian Y. AcrIIA5 inhibits a broad range of Cas9 orthologs by preventing DNA target cleavage. Cell Rep. 2019;29(2579–89):e4.
15. Cui YR, Wang SJ, Chen J, Li J, Chen W, Wang S, Meng B, Zhu W, Zhang Z, Yang B, et al. Allosteric inhibition of CRISPR-Cas9 by bacteriophage-derived peptides. Genome Biol. 2020;21:51.
16. Yang H, Patel DJ. Inhibition mechanism of an anti-CRISPR suppressor AcrIIA4 targeting SpyCas9. Mol Cell. 2017;67(117–27):e5.
17. Bubeck F, Hoffmann MD, Harteveld Z, Aschenbrenner S, Bietz A, Waldhauer MC, Borner K, Fakhiri J, Schmelas C, Dietz L, et al. Engineered anti-CRISPR proteins for optogenetic control of CRISPR-Cas9. Nat Methods. 2018;15:924–7.
18. Maji B, Gangopadhyay SA, Lee M, Shi M, Wu P, Heler R, Mok B, Lim D, Siriwardena SU, Paul B, et al. A high-throughput platform to identify small-molecule inhibitors of CRISPR-Cas9. Cell. 2019;177(1067–79):e19.
19. Lim D, Zhou Q, Cox KJ, Law BK, Lee M, Kokkonda P, Sreekanth V, Pergu R, Chaudhary SK, Gangopadhyay SA, et al. A general approach to identify cell-permeable and synthetic anti-CRISPR small molecules. Nat Cell Biol. 2022;24:1766–75.
20. Das A, Rai J, Roth MO, Shu Y, Medina ML, Barakat MR, Li H. Coupled catalytic states and the role of metal coordination in Cas9. Nat Catal. 2023;6:969–77.
21. Ishido T, Ishikawa M, Hirano K. Analysis of supercoiled DNA by agarose gel electrophoresis using low-conducting sodium threonine medium. Anal Biochem. 2010;400:148–50.
22. Shin J, Jiang F, Liu JJ, Bray NL, Rauch BJ, Baik SH, Nogales E, Bondy-Denomy J, Corn JE, Doudna JA. Disabling Cas9 by an anti-CRISPR DNA mimic. Sci Adv. 2017;3:e1701620.
23. Jiang F, Liu JJ, Osuna BA, Xu M, Berry JD, Rauch BJ, Nogales E, Bondy-Denomy J, Doudna JA. Temperature-responsive competitive inhibition of CRISPR-Cas9. Mol Cell. 2019;73:601-10.e5.
24. Foglesong PD, Reckord C, Swink S. Doxorubicin inhibits human DNA topoisomerase I. Cancer Chemother Pharmacol. 1992;30:123–5.
25. Bellosillo B, Colomer D, Pons G, Gil J. Mitoxantrone, a topoisomerase II inhibitor, induces apoptosis of B-chronic lymphocytic leukaemia cells. Br J Haematol. 1998;100:142–6.
26. Lehmann M, Vilar Kde S, Franco A, Reguly ML, Rodrigues de Andrade HH. Activity of topoisomerase inhibitors daunorubicin, idarubicin, and aclarubicin in the Drosophila somatic mutation and recombination test. Environ Mol Mutagen. 2004;43:250–7.
27. Thomas D, Hammerling BC, Wu K, Wimmer AB, Ficker EK, Kirsch GE, Kochan MC, Wible BA, Scholz EP, Zitron E, et al. Inhibition of cardiac HERG currents by the DNA topoisomerase II inhibitor amsacrine: mode of action. Br J Pharmacol. 2004;142:485–94.
28. Nitiss JL. Targeting DNA topoisomerase II in cancer chemotherapy. Nat Rev Cancer. 2009;9:338–50.
29. Bolzán AD, Bianchi MS. DNA and chromosome damage induced by bleomycin in mammalian cells: an update. Mutat Res Rev Mutat Res. 2018;775:51–62.
30. González RG, Haxo RS, Schleich T. Mechanism of action of polymeric aurintricarboxylic acid, a potent inhibitor of protein–nucleic acid interactions. Biochemistry. 1980;19:4299–303.
31. Wang X, Martindale JL, Holbrook NJ. Requirement for ERK activation in cisplatin-induced apoptosis. J Biol Chem. 2000;275:39435–43.
32. Meinelt T, Rose A, Pietrock M. Effects of calcium content and humic substances on the toxicity of acriflavine to juvenile ZebrafishDanio rerio. J Aquat Anim Health. 2002;14:35–8.
33. Vogtherr M, Grimme S, Elshorst B, Jacobs DM, Fiebig K, Griesinger C, Zahn R. Antimalarial drug quinacrine binds to C-terminal helix of cellular prion protein. J Med Chem. 2003;46:3563–4.

Zhang *et al. Genome Biology*   (2025) 26:75

Page 36 of 38

34. Kong D, Park EJ, Stephen AG, Calvani M, Cardellina JH, Monks A, Fisher RJ, Shoemaker RH, Melillo G. Echinomycin, a small-molecule inhibitor of hypoxia-inducible factor-1 DNA-binding activity. Cancer Res. 2005;65:9047–55.

35. Mori K, Schuettfort VM, Yanagisawa T, Katayama S, Pradere B, Laukhtina E, Rajwa P, Mostafaei H, Sari Motlagh R, Quhal F, et al. Reassessment of the efficacy of carboplatin for metastatic urothelial carcinoma in the era of immunotherapy: a systematic review and meta-analysis. Eur Urol Focus. 2022;8:1687–95.

36. Barret JM, Salles B, Provot C, Hill BT. Evaluation of DNA repair inhibition by antitumor or antibiotic drugs using a chemiluminescence microplate assay. Carcinogenesis. 1997;18:2441–5.

37. Drygin D, Lin A, Bliesath J, Ho CB, O'Brien SE, Proffitt C, Omori M, Haddach M, Schwaebe MK, Siddiqui-Jain A, et al. Targeting RNA polymerase I with an oral small molecule CX-5461 inhibits ribosomal RNA synthesis and solid tumor growth. Cancer Res. 2011;71:1418–30.

38. Nord CE, Rasmanis G, Wahlund E. Effect of dalbavancin on the normal intestinal microflora. J Antimicrob Chemother. 2006;58:627–31.

39. Wang Y, Feng J, Yu J, Wen L, Chen L, An H, Xiao W, Zhang B, Feng H, Zhou M, et al. Potent synergy and sustained bactericidal activity of polymyxins combined with Gram-positive only class of antibiotics versus four Gram-negative bacteria. Ann Clin Microbiol Antimicrob. 2024;23:60.

40. Palmeirim MS, Specht S, Scandale I, Gander-Meisterernst I, Chabicovsky M, Keiser J. Preclinical and clinical characteristics of the trichuricidal drug oxantel pamoate and clinical development plans: a review. Drugs. 2021;81:907–21.

41. Polnariev A. Antihistamines (H1 Receptor Antagonists). In: A worldwide yearly survey of new data in adverse drug reactions. 2015:185–94.

42. Duax WL, Ghosh D, Pletnev V. Steroid dehydrogenase structures, mechanism of action, and disease. Vitam Horm. 2000;58:121–48.

43. Fernando HA, Chandramouli C, Rosli D, Lam YL, Yong ST, Yaw HP, Ton SH, Kadir KA, Sainsbury A. Glycyrrhizic acid can attenuate metabolic deviations caused by a high-sucrose diet without causing water retention in male Sprague-Dawley rats. Nutrients. 2014;6:4856–71.

44. Seo HW, Seo JP, Cho Y, Ko E, Kim YJ, Jung G. Cetylpyridinium chloride interaction with the hepatitis B virus core protein inhibits capsid assembly. Virus Res. 2019;263:102–11.

45. Ibrar I, Yadav S, Altaee A, Safaei J, Samal AK, Subbiah S, Millar G, Deka P, Zhou J. Sodium docusate as a cleaning agent for forward osmosis membranes fouled by landfill leachate wastewater. Chemosphere. 2022;308:136237.

46. Oliver CL, Bauer JA, Wolter KG, Ubell ML, Narayan A, O'Connell KM, Fisher SG, Wang S, Wu X, Ji M, et al. In vitro effects of the BH3 mimetic, (-)-gossypol, on head and neck squamous cell carcinoma cells. Clin Cancer Res. 2004;10:7757–63.

47. Garcia N, Zazueta C, Pavon N, Chavez E. Agaric acid induces mitochondrial permeability transition through its interaction with the adenine nucleotide translocase. Its dependence on membrane fluidity. Mitochondrion. 2005;5:272–81.

48. Tominari T, Matsumoto C, Watanabe K, Hirata M, Grundler FM, Miyaura C, Inada M. Epigallocatechin gallate (EGCG) suppresses lipopolysaccharide-induced inflammatory bone resorption, and protects against alveolar bone loss in mice. FEBS Open Bio. 2015;5:522–7.

49. Liu T, Yang Q, Zhang X, Qin R, Shan W, Zhang H, Chen X. Quercetin alleviates kidney fibrosis by reducing renal tubular epithelial cell senescence through the SIRT1/PINK1/mitophagy axis. Life Sci. 2020;257:118116.

50. Goldim MPS, Della Giustina A, Petronilho F. Using evans blue dye to determine blood-brain barrier integrity in rodents. Curr Protoc Immunol. 2019;126:e83.

51. Burkhardt H, Rosenthal S, Rosenthal HA, Karge E, De Clercq E. Treatment of bovine leukaemia virus-infected sheep with suramin: an animal model for the development of antiretroviral compounds. Acta Virol. 1989;33:305–13.

52. Milne JC, Lambert PD, Schenk S, Carney DP, Smith JJ, Gagne DJ, Jin L, Boss O, Perni RB, Vu CB, et al. Small molecule activators of SIRT1 as therapeutics for the treatment of type 2 diabetes. Nature. 2007;450:712–6.

53. Clave P, Acalovschi M, Triantafillidis JK, Uspensky YP, Kalayci C, Shee V, Tack J, Investigators OS. Randomised clinical trial: otilonium bromide improves frequency of abdominal pain, severity of distention and time to relapse in patients with irritable bowel syndrome. Aliment Pharmacol Ther. 2011;34:432–42.

54. Coldewey SM, Benetti E, Collino M, Pfeilschifter J, Sponholz C, Bauer M, Huwiler A, Thiemermann C. Elevation of serum sphingosine-1-phosphate attenuates impaired cardiac function in experimental sepsis. Sci Rep. 2016;6:27594.

55. Yin W, Luan X, Li Z, Zhou Z, Wang Q, Gao M, Wang X, Zhou F, Shi J, You E, et al. Structural basis for inhibition of the SARS-CoV-2 RNA polymerase by suramin. Nat Struct Mol Biol. 2021;28:319–25.

56. Cersosimo RJ, Hong WK. Epirubicin: a review of the pharmacology, clinical activity, and adverse effects of an adriamycin analogue. J Clin Oncol. 1986;4:425–39.

57. Malabarba A, Nicas TI, Thompson RC. Structural modifications of glycopeptide antibiotics. Med Res Rev. 1997;17:69–137.

58. Nishimasu H, Cong L, Yan WX, Ran FA, Zetsche B, Li Y, Kurabayashi A, Ishitani R, Zhang F, Nureki O. Crystal structure of Staphylococcus aureus Cas9. Cell. 2015;162:1113–26.

59. Nelson JW, Randolph PB, Shen SP, Everette KA, Chen PJ, Anzalone AV, An M, Newby GA, Chen JC, Hsu A, et al. Engineered pegRNAs improve prime editing efficiency. Nat Biotechnol. 2022;40:402–10.

60. Ma E, Harrington LB, O'Connell MR, Zhou K, Doudna JA. Single-stranded DNA cleavage by divergent CRISPR-Cas9 enzymes. Mol Cell. 2015;60:398–407.

61. Scott DA, Zhang F. Implications of human genetic variation in CRISPR-based therapeutic genome editing. Nat Med. 2017;23:1095–101.

62. Walton RT, Christie KA, Whittaker MN, Kleinstiver BP. Unconstrained genome targeting with near-PAMless engineered CRISPR-Cas9 variants. Science. 2020;368:290–6.

63. Li SY, Cheng QX, Liu JK, Nie XQ, Zhao GP, Wang J. CRISPR-Cas12a has both cis- and trans-cleavage activities on single-stranded DNA. Cell Res. 2018;28:491–3.

Zhang *et al. Genome Biology*   (2025) 26:75

Page 37 of 38

64. Jiang Y, Chen B, Duan C, Sun B, Yang J, Yang S. Multigene editing in the Escherichia coli genome via the CRISPR-Cas9 system. Appl Environ Microbiol. 2015;81:2506–14.

65. Spallarossa A, Forlani F, Carpen A, Armirotti A, Pagani S, Bolognesi M, Bordo D. The "rhodanese" fold and catalytic mechanism of 3-mercaptopyruvate sulfurtransferases: crystal structure of SseA from Escherichia coli. J Mol Biol. 2004;335:583–93.

66. Brinkman EK, Chen T, Amendola M, van Steensel B. Easy quantitative assessment of genome editing by sequence trace decomposition. Nucleic Acids Res. 2014;42:e168.

67. Hill JT, Demarest BL, Bisgrove BW, Su YC, Smith M, Yost HJ. Poly peak parser: method and software for identification of unknown indels using sanger sequencing of polymerase chain reaction products. Dev Dyn. 2014;243:1632–6.

68. Shin J, Lee N, Cho S, Cho BK. Targeted genome editing using DNA-Free RNA-guided Cas9 ribonucleoprotein for CHO cell engineering. Methods Mol Biol. 2018;1772:151–69.

69. Hsu PD, Scott DA, Weinstein JA, Ran FA, Konermann S, Agarwala V, Li Y, Fine EJ, Wu X, Shalem O, et al. DNA targeting specificity of RNA-guided Cas9 nucleases. Nat Biotechnol. 2013;31:827–32.

70. Koblan LW, Doman JL, Wilson C, Levy JM, Tay T, Newby GA, Maianti JP, Raguram A, Liu DR. Improving cytidine and adenine base editors by expression optimization and ancestral reconstruction. Nat Biotechnol. 2018;36:843–6.

71. Jia K, Lu Z, Zhou F, Xiong Z, Zhang R, Liu Z, Ma Y, He L, Li C, Zhu Z, et al. Multiple sgRNAs facilitate base editing-mediated i-stop to induce complete and precise gene disruption. Protein Cell. 2019;10:832–9.

72. Tsai SQ, Zheng Z, Nguyen NT, Liebers M, Topkar VV, Thapar V, Wyvekens N, Khayter C, Iafrate AJ, Le LP, et al. GUIDE-seq enables genome-wide profiling of off-target cleavage by CRISPR-Cas nucleases. Nat Biotechnol. 2015;33:187–97.

73. Mangeot PE, Risson V, Fusil F, Marnef A, Laurent E, Blin J, Mournetas V, Massouridès E, Sohier TJM, Corbin A, et al. Genome editing in primary cells and in vivo using viral-derived Nanoblades loaded with Cas9-sgRNA ribonucleoproteins. Nat Commun. 2019;10:45.

74. Ibraheim R, Song CQ, Mir A, Amrani N, Xue W, Sontheimer EJ. All-in-one adeno-associated virus delivery and genome editing by Neisseria meningitidis Cas9 in vivo. Genome Biol. 2018;19:137.

75. Yin H, Xue W, Chen S, Bogorad RL, Benedetti E, Grompe M, Koteliansky V, Sharp PA, Jacks T, Anderson DG. Genome editing with Cas9 in adult mice corrects a disease mutation and phenotype. Nat Biotechnol. 2014;32:551–3.

76. Zhang L, Wang L, Xie Y, Wang P, Deng S, Qin A, Zhang J, Yu X, Zheng W, Jiang X. Triple-targeting delivery of CRISPR/Cas9 to reduce the risk of cardiovascular diseases. Angew Chem Int Ed Engl. 2019;58:12404–8.

77. Zuo Z, Liu J. Allosteric regulation of CRISPR-Cas9 for DNA-targeting and cleavage. Curr Opin Struct Biol. 2020;62:166–74.

78. Ivanov IE, Wright AV, Cofsky JC, Aris KDP, Doudna JA, Bryant Z. Cas9 interrogates DNA in discrete steps modulated by mismatches and supercoiling. Proc Natl Acad Sci U S A. 2020;117:5853–60.

79. Newton MD, Losito M, Smith QM, Parnandi N, Taylor BJ, Akcakaya P, Maresca M, van Eijk P, Reed SH, Boulton SJ, et al. Negative DNA supercoiling induces genome-wide Cas9 off-target activity. Mol Cell. 2023;83:3533-45.e5.

80. Shi YJ, Duan M, Ding JM, Wang FQ, Bi LL, Zhang CX, Zhang YZ, Duan JY, Huang AH, Lei XL, et al. DNA topology regulates PAM-Cas9 interaction and DNA unwinding to enable near-PAMless cleavage by thermophilic Cas9. Mol Cell. 2022;82(4160–75):e6.

81. Reagan-Shaw S, Nihal M, Ahmad N. Dose translation from animal to human studies revisited. FASEB J. 2008;22:659–61.

82. Békés M, Langley DR, Crews CM. PROTAC targeted protein degraders: the past is prologue. Nat Rev Drug Discov. 2022;21:181–200.

83. Pommier Y. Drugging topoisomerases: lessons and challenges. ACS Chem Biol. 2013;8:82–95.

84. Pommier Y, Marchand C. Interfacial inhibitors: targeting macromolecular complexes. Nat Rev Drug Discov. 2011;11:25–36.

85. Mackenzie CD. The safety of pyrantel, oxantel, and morantel. In: Marchiondo AA, editor. Pyrantel parasiticide therapy in humans and domestic animals. London: Academic Press. 2016:47–66.

86. Pindado S, Corriganh OI, O'Driscoll CM. Carbenoxolone sodium. 1996:1–43.

87. Vrignaud P, Eghbali H, Hoerni B, Iliadis A, Robert J. Pharmacokinetics and metabolism of epirubicin during repetitive courses of administration in Hodgkin's patients. Eur J Cancer Clin Oncol. 1985;21:1307–13.

88. Zhanel GG, Calic D, Schweizer F, Zelenitsky S, Adam H, Lagacé-Wiens PR, Rubinstein E, Gin AS, Hoban DJ, Karlowsky JA. New lipoglycopeptides: a comparative review of dalbavancin, oritavancin and telavancin. Drugs. 2010;70:859–86.

89. Lobo E. A study to evaluate the pharmacokinetics of pamoic acid following oral administration as hydroxyzine pamoate (Vistaril®) in healthy male subjects. Clin Pharmacol Ther. 2006;PIII-76:P79.

90. Gagnon JA, Valen E, Thyme SB, Huang P, Akhmetova L, Pauli A, Montague TG, Zimmerman S, Richter C, Schier AF. Efficient mutagenesis by Cas9 protein-mediated oligonucleotide insertion and large-scale assessment of single-guide RNAs. PLoS One. 2014;9:e98186.

91. Soares Medeiros LC, South L, Peng D, Bustamante JM, Wang W, Bunkofske M, Perumal N, Sanchez-Valdez F, Tarleton RL. Rapid, selection-free, high-efficiency genome editing in protozoan parasites using CRISPR-Cas9 ribonucleoproteins. mBio. 2017;8:e01788.

92. Croppi G, Zhou Y, Yang R, Bian Y, Zhao M, Hu Y, Ruan BH, Yu J, Wu F. Discovery of an inhibitor for bacterial 3-mercaptopyruvate sulfurtransferase that synergistically controls bacterial survival. Cell Chem Biol. 2020;27:1483-99.e9.

93. Shong J, Huang YM, Bystroff C, Collins CH. Directed evolution of the quorum-sensing regulator EsaR for increased signal sensitivity. ACS Chem Biol. 2013;8:789–95.

94. Ran FA, Hsu PD, Wright J, Agarwala V, Scott DA, Zhang F. Genome engineering using the CRISPR-Cas9 system. Nat Protoc. 2013;8:2281–308.

95. Lu Y, Wan J, Yang Z, Lei X, Niu Q, Jiang L, Passtoors WM, Zang A, Fraering PC, Wu F. Regulated intramembrane proteolysis of the AXL receptor kinase generates an intracellular domain that localizes in the nucleus of cancer cells. FASEB J. 2017;31:1382–97.

Zhang *et al. Genome Biology*   (2025) 26:75

Page 38 of 38

96. Peng D, Tarleton R. EuPaGDT: a web tool tailored to design CRISPR guide RNAs for eukaryotic pathogens. Microb Genom. 2015;1:e000033.
97. Concordet JP, Haeussler M. CRISPOR: intuitive guide selection for CRISPR/Cas9 genome editing experiments and screens. Nucleic Acids Res. 2018;46:W242–5.
98. Hu Y, Wang L, Han X, Zhou Y, Zhang T, Wang L, Hong T, Zhang W, Guo XX, Sun J, et al. Discovery of a bioactive inhibitor with a new scaffold for cystathionine γ-lyase. J Med Chem. 2019;62:1677–83.
99. Aldrich C, Bertozzi C, Georg GI, Kiessling L, Lindsley C, Liotta D, Merz KM Jr, Schepartz A, Wang S. The ecstasy and agony of assay interference compounds. J Med Chem. 2017;60:2165–8.
100. Zhao C, Dodin G, Yuan C, Chen H, Zheng R, Jia Z, Fan BT. "In vitro" protection of DNA from Fenton reaction by plant polyphenol verbascoside. Biochim Biophys Acta. 2005;1723:114–23.
101. Shatalin K, Shatalina E, Mironov A, Nudler E. H2S: a universal defense against antibiotics in bacteria. Science. 2011;334:986–90.
102. Pinder J, Salsman J, Dellaire G. Nuclear domain "knock-in" screen for the evaluation and identification of small molecule enhancers of CRISPR-based genome editing. Nucleic Acids Res. 2015;43:9379–92.
103. Wu CC, Li YC, Wang YR, Li TK, Chan NL. On the structural basis and design guidelines for type II topoisomerase-targeting anticancer drugs. Nucleic Acids Res. 2013;41:10630–40.
104. Bravo JPK, Liu MS, Hibshman GN, Dangerfield TL, Jung K, McCool RS, Johnson KA, Taylor DW. Structural basis for mismatch surveillance by CRISPR-Cas9. Nature. 2022;603:343–7.
105. Mamar H, Fajka-Boja R, Mórocz M, Jurado EP, Zentout S, Mihuţ A, Kopasz AG, Mérey M, Smith R, Sharma AB, et al. The loss of DNA polymerase epsilon accessory subunits POLE3-POLE4 leads to BRCA1-independent PARP inhibitor sensitivity. Nucleic Acids Res. 2024;52:6994–7011.
106. Zhang X, Xu C, Gao S, Li P, Kong Y, Li T, Li Y, Xu FJ, Du J. CRISPR/Cas9 delivery mediated with hydroxyl-rich nanosystems for gene editing in Aorta. Adv Sci (Weinh). 2019;6:1900386.
107. Liu F, Song Y, Liu D. Hydrodynamics-based transfection in animals by systemic administration of plasmid DNA. Gene Ther. 1999;6:1258–66.
108. Clement K, Rees H, Canver MC, Gehrke JM, Farouni R, Hsu JY, Cole MA, Liu DR, Joung JK, Bauer DE, et al. CRISPResso2 provides accurate and rapid genome editing sequence analysis. Nat Biotechnol. 2019;37:224–6.

Publisher's Note